

CHARACTERIZATION OF ELECTRODEPOSITED
CdTe PREPARED UNDER DIFFERENT
CONDITIONS

ARTHUR LAKES LIBRARY
COLORADO SCHOOL OF MINES
GOLDEN, CO 80401

by
Esam Alarfaj

ProQuest Number: 10794237

All rights reserved

INFORMATION TO ALL USERS

The quality of this reproduction is dependent upon the quality of the copy submitted.

In the unlikely event that the author did not send a complete manuscript and there are missing pages, these will be noted. Also, if material had to be removed, a note will indicate the deletion.



ProQuest 10794237

Published by ProQuest LLC (2018). Copyright of the Dissertation is held by the Author.

All rights reserved.


This work is protected against unauthorized copying under Title 17, United States Code
Microform Edition © ProQuest LLC.

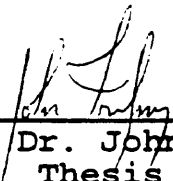
ProQuest LLC.
789 East Eisenhower Parkway
P.O. Box 1346
Ann Arbor, MI 48106 – 1346

A thesis submitted to the Faculty and Board of Trustees
of the Colorado School of Mines in partial fulfilment of the
requirements for the degree of Master of Science (Physics).

Golden, Colorado


Date 11/4/96

Signed: 
Esam Alarfaj

Approved: 
Dr. John Trefny
Thesis Advisor

Golden, Colorado

Date 11/4/96


Dr. Don L. Williamson
Professor and Head
Department of Physics

ABSTRACT

The effects of changing deposition potential on the optical and structural properties of CdTe grown on CdS/SnO₂/glass substrates have been investigated using X-ray diffraction (XRD), photoluminescence, scanning electron microscopy (SEM), and Auger electron spectroscopy (AES) techniques.

X-ray diffraction was employed to investigate the texture of the CdTe thin films. It was observed that all as-grown samples have a strong preferred orientation in the [111] direction, but with different strengths. However, after annealing, the [220] direction becomes the dominant direction in most samples, also with different strengths.

Photoluminescence was employed to determine the band gaps of the different samples and to try to correlate them to interdiffusion. Photoluminescence was also used to obtain information about defect levels in the samples.

Auger electron spectroscopy was employed to study interdiffusion at the CdTe/CdS interface and deep into the respective layers. It was observed that different samples had different degrees of interdiffusion both at the

interface and inside the layers. A novel technique was used to study interdiffusion in the different layers in addition to the interface.

The results of both techniques were consistent and confirmed previous study at CSM on the interdiffusion using XRD. All studies confirmed the penetration of S into the CdTe layer and Te into the CdS layer in the standard deposition potential sample. However this study shows that the interdiffusion is less at other deposition potentials. Finally, we have attempted to correlate this result to the morphology of the different samples.

TABLE OF CONTENTS

	Page
ABSTRACT-----	iii
TABLE OF CONTENTS-----	v
LIST OF FIGURES-----	vii
LIST OF TABLES-----	x
ACKNOWLEDGMENTS-----	xi
CHAPTER 1. INTRODUCTION-----	1
CHAPTER 2. ELECTRODEPOSITION OF CdTe-----	7
2-1. The apparatus-----	8
2-2. The voltammogram-----	10
CHAPTER 3. TECHNIQUES-----	20
3-1. X-ray Diffraction-----	20
3-1.1. Determination of Texture-----	20
3-1.2. Grain Size-----	23
3-2. Photoluminescence Measurements-----	24
3-3. Scanning Electron Microscopy (SEM)-----	26
3-4. Auger Electron Spectroscopy-----	27
3-5. Hot Probe-----	28
CHAPTER 4. EXPERIMENTAL DETAILS-----	30
4-1. Sample Preparation-----	30
4-2. X-ray Diffraction-----	31
4-3. Auger Electron Spectroscopy-----	31
4-3.1. Depth Profiling by Ion Sputtering-----	32
4-3.2. Depth Profiling by Mechanical Polishing-----	33
4-4. Photoluminescence-----	36

4-5.Efficiency Measurements-----	37
CHAPTER 5.RESULTS AND DISCUSSION-----	39
5-1.Hot Probe Measurements -----	39
5-2.X-ray Diffraction-----	39
5-2.1.Texture-----	39
5-2.2.Grain Size-----	55
5-3.Scanning Electron Microscopy(SEM)-----	55
5-4.Photoluminescence-----	61
5-5.Lifetime Measurements-----	71
5-6.Auger Electron Spectroscopy-----	72
5-7.Efficiency Measurements-----	81
CHAPTER 6.SUMMARY AND CONCLUSION-----	82
REFERENCES CITED-----	84

LIST OF FIGURES

Fig. 1.1.Theoretical efficiencies of absorber materials-----	4
Fig. 1.2.Cross section of solar cell-----	5
Fig. 2.1.Schematic of CdTe electrodeposition apparatus.----	9
Fig. 2.2.Voltammogram for deposition of CdTe-----	13
Fig. 2.3.Diagram of the reaction regions near the cathode-	15
Fig. 2.4.Voltammogram of CdTe from Panicker et al.-----	17
Fig 2.5.Voltammogram of CdTe from Takahashi et al.-----	18
Fig. 3.1.Schematic cross section Of polycrystalline thin film-----	22
Fig. 3.2.Radiative transitions observed with PL-----	27
Fig. 3.3.Schematic diagram for the hot probe set up -----	29
Fig. 4.1.The depth resolution for films evaporated along the surface normal for rough substrate subsequently sputtered with ions at an angle β from the surface normal -----	34
Fig. 4.2.Cross section of mechanically polished sample----	36
Fig. 4.3.Apparatus used for photoluminescence measurement -----	38
Fig. 5.1.XRD pattern of powder CdTe-----	41
Fig. 5.2.XRD pattern of as deposited CdTe (sample 46-6)---	43
Fig. 5.3.XRD of Annealed CdTe (sample 46-6) -----	45
Fig. 5.4.XRD pattern of As-deposited CdTe (sample 46-5----	47
Fig. 5.5.XRD pattern of Annealed CdTe (sample 46-5) -----	48
Fig. 5.6.XRD pattern of as-grown CdTe (sample 46-3) -----	50

Fig. 5.7.XRD pattern of Annealed CdTe (sample 46-3)	-----51
Fig. 5.8.XRD pattern of as-grown CdTe(sample 82-2)	-----53
Fig. 5.9.XRD pattern of annealed CdTe (sample 82-2)	-----54
Fig. 5.10.Topography of annealed CdTe 46-3	-----58
Fig. 5.11.Topography of annealed CdTe 46-5	-----59
Fig. 5.12.Topography of annealed CdTe 82-2	-----60
Fig. 5.13.A typical PL intensity spectrum of CdTe at 77 K	61
Fig. 5.14.Optical energy gap of CdS _x Te _{1-x} at 300K and at 100 K	-----63
Fig. 5.15.PL measurements of as-grown CdTe 46-5	-----65
Fig. 5.16.PL measurements of as-grown CdTe sample 46-6	---65
Fig. 5.17.PL measurements of as-grown CdTe 46-6 20 sec exposure.	-----66
Fig. 5.18.PL measurements of as-grown CdTe 46-3	-----66
Fig. 5.19.PL measurements of annealed CdTe 46-5 at room temperature.	-----67
Fig. 5.20.PL measurements of annealed CdTe 46-6 at room temperature	-----67
Fig. 5.21.PL measurements of annealed CdTe 46-3 at room temperature.	-----68
Fig. 5.22.PL measurements of annealed CdTe 46-5 at 5K	-----68
Fig. 5.23.PL measurements of annealed CdTe 46-3 at 5K	-----69
Fig. 5.24.PL measurements of annealed CdTe 46-6 at 5K	-----69
Fig. 5.25.Lifetimes of the three samples of CdTe.	-----71
Fig. 5.26.line scan of the as-grown sample 46-5.	-----74
Fig. 5.27.Cd peak in the CdTe region for as-grown 46-5	----74

Fig. 5.28.Cd peak in the CdS region for as-grown 46-5-----	75
Fig. 5.29.Cd peak in the interface for as-grown 46-5-----	75
Fig. 5.30.Cd peak in the CdTe region for annealed 46-5----	76
Fig. 5.31.Cd peak in the interface for annealed 46-5 -----	76
Fig. 5.32.Line scan for annealed 46-5 -----	77
Fig. 5.33.Line scan for as-grown 46-6 -----	77
Fig. 5.34.Cd peak in the interface for as-grown 46-6 -----	78
Fig. 5.35.Cd peak in the CdTe region for as-grown 46-6 ---	78
Fig. 5.36.Cd peak in the CdS region for as-grown 46-6 ----	79
Fig. 5.37.Cd peak in the CdTe region for annealed 46-6 ---	79
Fig. 5.38.Cd peak in the CdS region for annealed 46-6 ----	80
Fig. 5.39.Cd peak in the interface for annealed 46-6 -----	80

LIST OF TABLES

	Page
Table 4.1 Deposition potentials of CdTe samples. -----	30
Table 4.2 Variable potential deposition data(82-2)-----	31
Table 5.1 Calculation of integrated intensities of powder CdTe-----	40
Table 5.2 Measured integrated intensities of powder CdTe--	41
Table 5.3 Integrated intensities of as grown CdTe 46-6 ---	43
Table 5.4 XRD pattern of annealed CdTe (sample 46-6) -----	45
Table 5.5 XRD pattern of as-deposited CdTe sample 46-5 ---	47
Table 5.6 XRD pattern of annealed 46-5 -----	48
Table 5.7 XRD pattern of as-deposited 46-3 -----	50
Table 5.8 XRD pattern of annealed CdTe (sample 46-3) -----	51
Table 5.9 XRD pattern of as-grown CdTe (sample 82-2)-----	53
Table 5.10 XRD pattern of annealed CdTe (sample 82-2)-----	54
Table 5.11 Calculated grain sizes of as deposited CdTe----	56
Table 5.12 Calculated grain sizes of annealed CdTe -----	56
Table 5.13 Grain size for annealed CdTe. -----	57
Table 5.14 Efficiencies of the different samples of CdTe--	81

ACKNOWLEDGMENTS

I wish to take this opportunity to express my gratitude to a number of individuals.

Professor John Trefny, my thesis advisor, for his advice, guidance, and encouragement. I learned a lot from his patient and quiet way of dealing with things. Professor Don Williamson for his support and suggestions of X-ray diffraction studies. Professor Reuben Collins for his suggestions and advice.

Thanks goes to Dr. Tim Ohno, Art Nelson, and Ahmet Balcioglu for the AES measurements and discussions. Thanks goes to the rest of CdTe group and my fellow graduate students Jian Tang and Wenjie Song.

Thanks also goes to Professor Fuad Abulfotouh of NREL for doing the PL measurements and for discussions.

Finally thanks goes to my family for their understanding and support.

CHAPTER ONE

INTRODUCTION

Is there any real requirement for another source of energy? To answer this question, various issues and questions regarding current sources of energy must be considered. How long each source will last, the rate of energy that can be obtained from that source, and the cost of energy all must be taken into consideration in answering this question. As the population of humans increases, their consumption of energy will increase too, so they must make sure that a dependable source of energy is available.

Considering conventional energy supplies, oil is a major source nowadays. Furthermore, it is a fluid that can be easily transported. However, we have to think of other sources of energy not only because the world reserves of oil and other fuels are limited and one day will be depleted, but also because amounts of fuels have many other vital applications, ranging from fertilizers to pharmaceuticals, and one day oil must be kept for these applications only, since other sources might do the primary job of providing energy. Coal is the most plentiful fossil fuel energy.

However, it is not easy to transport and causes a lot of pollution to the environment when it is burned.

Nuclear fission can provide energy for a long time; however it has some disadvantages. The waste of nuclear fission is radioactive with half lives extending to tens of thousands of years. Storage of these wastes still is a real concern for our societies. Also reactor accidents represent a real worry for the public. Ten Mile Island and Chernobyl are just two examples of how dangerous these reactors might be.

Among all these concerns, solar energy emerges as a distinctive and promising source. It takes part indirectly in the creation of other conventional sources of energy like coal, oil, and natural gas. Solar energy can be used either for heating and cooling in the form of solar thermal energy, or it can be used to produce electricity directly. About 10% of the world's energy requirements can be met using solar thermal energy[1]. An important use of solar energy, though, is solar cells which convert sunlight into electricity directly. This way is preferred because electricity is extremely advantageous. It can be easily transported and converted into other forms of energy. It also can be stored in many ways: electrical energy in the form of SMES (superconducting magnetic energy storage) or in

a capacitor, as potential energy, or in the form of chemical energy (battery). Despite all of its advantages, however, most energy experts do not expect that solar energy will be the major source of power in the twenty-first century.

The French scientist Edmund Becquerel discovered the photovoltaic effect in 1839 [2]. Charles Fritts was the first to invent a practical solar cell made from selenium [2]. Nevertheless, the major development was in 1950 at Bell Laboratories. Cal Faller, Darryl Chapin and Gordon Pearson produced a silicon cell with an efficiency of 4% [2]. By 1954 they reached 6% efficiency. Later, the US space program helped to promote research on photovoltaics. In 1973, the oil crisis gave a boost to research in solar cells. The side effects of conventional sources of energy like air and water pollution, supply crises, international tension, resource depletion and fear of nuclear accidents are all factors that add up to encourage research in photovoltaics as a substitute. Recently, the concern over the greenhouse effect has brought new attention to photovoltaics. Although international tension is a side effect in the conventional sources of energy, it may come about in a new form in the case of solar power since most of the sunshine is intensified in the developing countries rather than the industrial countries.

CdTe solar cells have the highest potential for low cost manufacturing and high efficiency. Interest in CdTe started about 35 years ago; it was an interesting material since its bandgap of 1.5 eV is ideally matched to the solar spectrum(see Figure 1.1). This bandgap is at the maximum in terms of its potential for high efficiency as a single junction device [3].

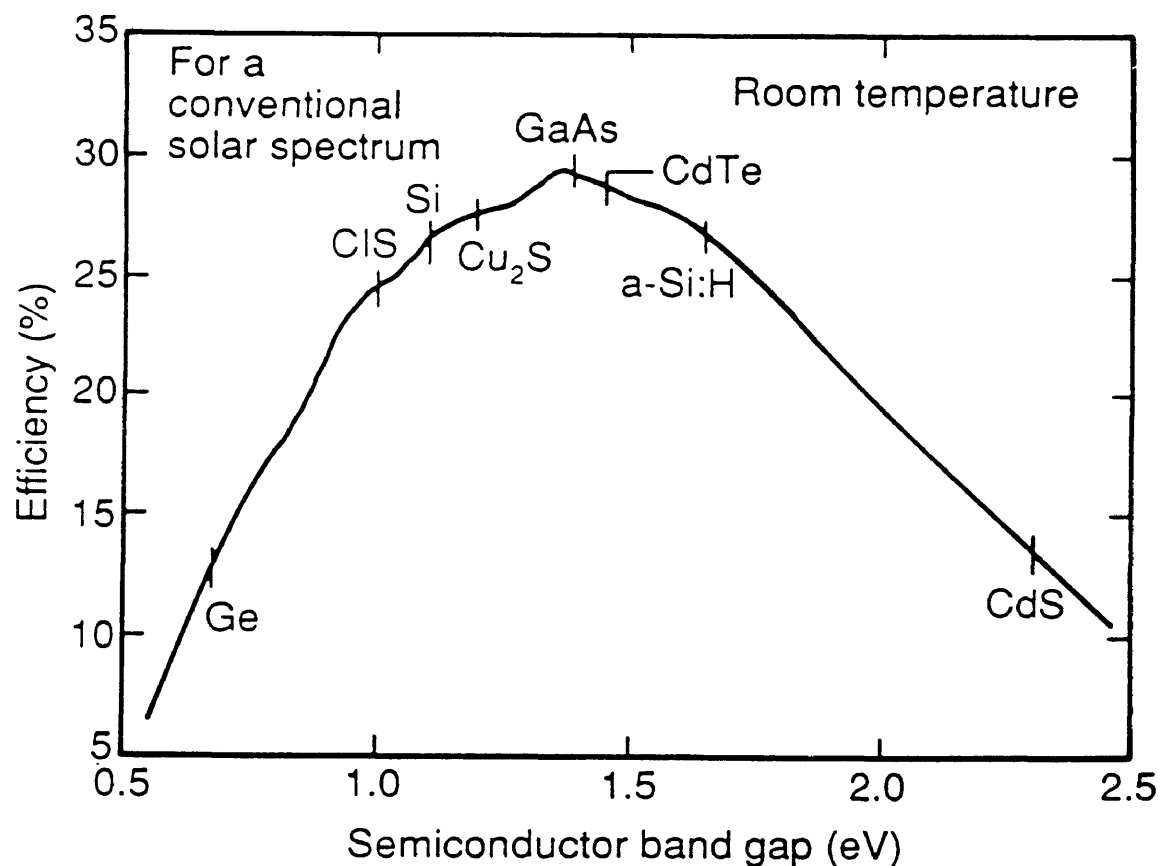


Fig. 1.1 Theoretical efficiencies of a single junction solar cell or a junction of band gap of the absorber materials[3].

A CdTe solar cell was first reported in 1972 by D. Bonnet et al. [3]. It has many advantages: it may be the most inexpensive to make, also it can be fabricated by a variety of low cost methods; it also has one of the highest absorption coefficients of any photovoltaic material ranging between $10^4/\text{cm}$ - $10^5/\text{cm}$. This implies that only 1-2 μm is sufficient to absorb all of the incident light. On the other hand, it has some disadvantages such as the potentially hazardous effects of cadmium.

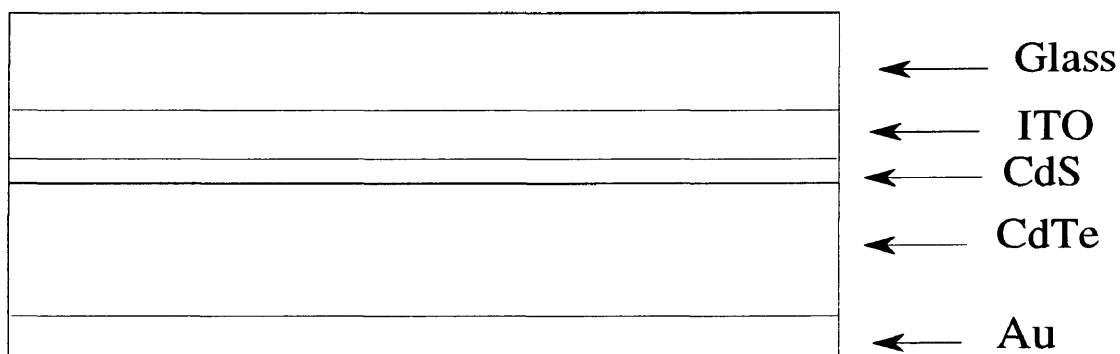


Fig. 1.2 Schematic cross section of solar cell

In this work, the effects of different deposition potentials on the properties of CdTe thin films prepared by electrodeposition were studied. Fig. 1.2 exhibits a typical structure of a modern CdTe solar cell such as those prepared for this study. The microstructure and texture of the films

were investigated using x-ray diffraction techniques and scanning electron microscopy (SEM). The nature of the physical junction between CdTe and CdS was studied using Auger spectroscopy. Optical properties were studied using photoluminescence techniques.

CHAPTER 2

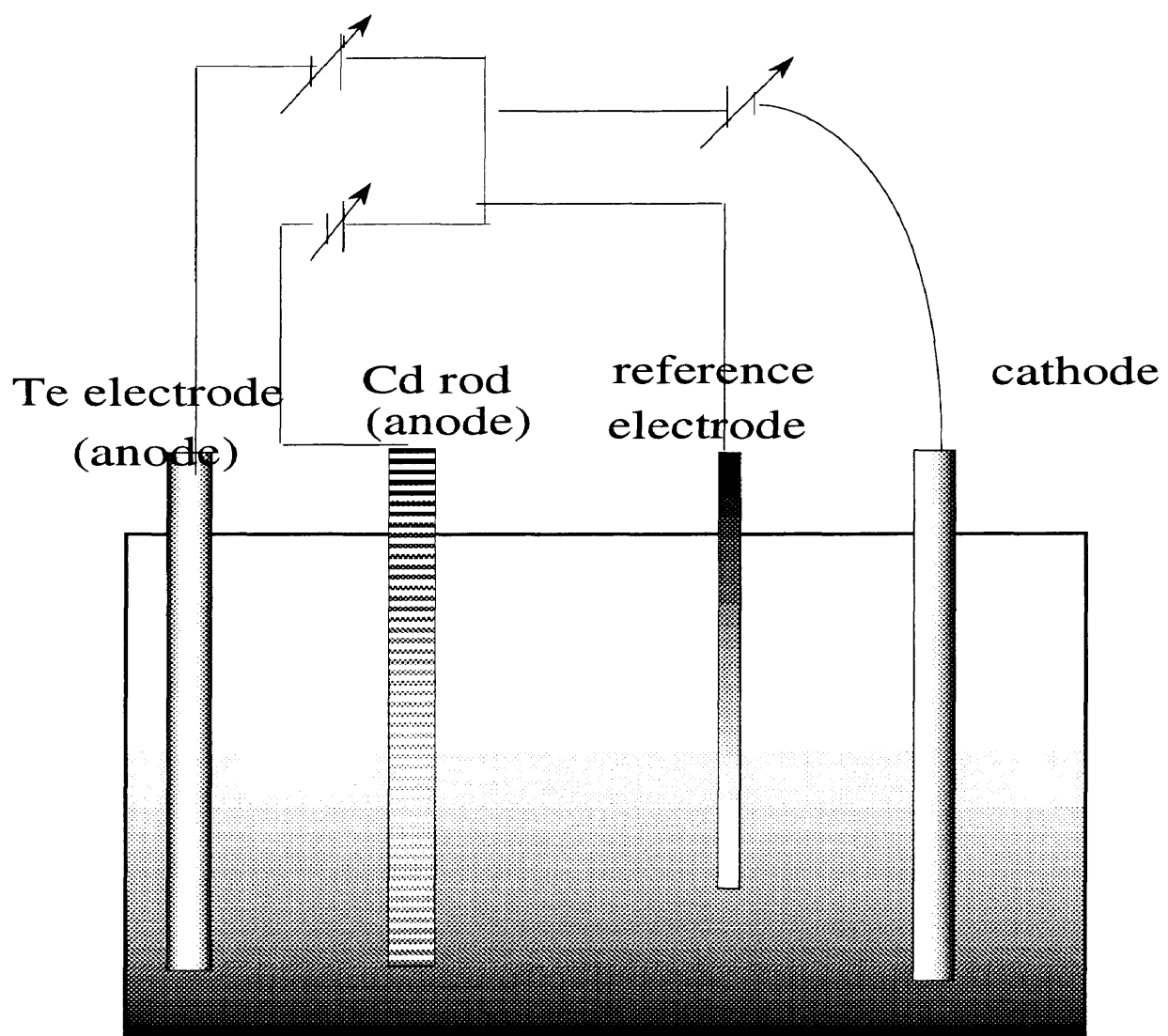
ELECTRODEPOSITION OF CdTe

Electrodeposition is a method by which a material is deposited from an electrolyte onto a substrate due to the flow of an ionic electric current. It has many advantages over other deposition methods. For example, it is a low temperature process in which low cost substrates, like soda lime glass, can be used. Also, as a low temperature process, it can minimize problems of cross diffusion of dopants. It can be scaled up for industrial mass production. It also can be used to directly deposit either p-type or n-type CdTe. Furthermore, there is no waste of materials since deposition takes place only on a selected area, so that almost every Cd or Te atom ends up in CdTe. In addition, good, uniform films free of pinholes are obtained. Finally, it is also a low cost process, since the equipment needed to accomplish it is very inexpensive. Its primary disadvantage for CdTe deposition is that it is a slow process. It takes about one hour to make a film of one micron thickness. However, this characteristic can also be

considered as an advantage since it allows good control of thin films.

2-1. The apparatus

The solar cell equipment and technology used at CSM was developed by Ametek and donated to CSM in 1992. A 30 liter bath containing 1.2 M CdCl_2 and 20-30 ppm Te was used in this work. Four electrodes were immersed in the bath (see Figure 2.1): two anodes, a cathode and a reference electrode. A cadmium rod and platinized basket containing small diameter Te pellets (2 mm diameter) were the two anodes, and the cathode was either the substrate or platinum mesh. The reference electrode was Ag/AgCl. The concentration of Cd was kept at 1.2 M by adding CdCl_2 when needed. The pH was kept at 2 by adding drops of HCl when the pH rose. The temperature was kept at 80°C . A schematic of a deposition system is shown in Fig. 2.1.



Simplified schematic diagram of the bath in which CdTe is deposited

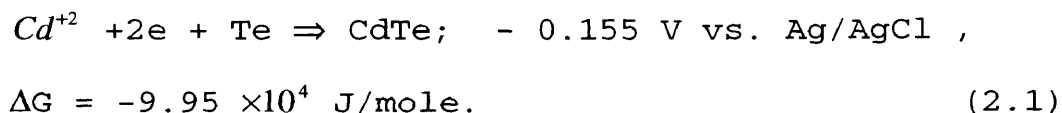
Fig.2.1 Diagram of CdTe deposition bath.

2-2. The Voltammogram

According to Panicker et al.[4], CdTe can be deposited in a range of potentials starting from CdTe in equilibrium with Cd to CdTe in equilibrium with Te. In this range, the Cd activity changes from $a_{cd} = 1$ at the CdTe/Cd boundary to $a_{cd} = \exp(G_{CdTe}/RT)$ at the CdTe/Te boundary, where G_{CdTe} is the Gibbs free energy of the reaction. Also, the Te activity varies from $a_{Te} = 1$ at the CdTe /Te boundary to $a_{Te} = \exp(G_{CdTe}/RT)$ at the CdTe/Cd boundary. So, the compound formation causes a shift in the cadmium potential from a standard potential value of -0.603 V vs. Ag/AgCl at the CdTe/Cd boundary to -0.057 V vs. Ag/AgCl. Additionally, the Te potential shifts from a standard potential value of .351 V vs. Ag/AgCl to 0.624 V [4].

Since Cd is the potential determining species, CdTe can be deposited from $V_{dep} = -.603 + .295 \log a_{cd+2} - \Delta V$ to $V_{dep} = -0.057 + 0.295 \log a_{cd+2} - \Delta V$ where: $\Delta V = \eta + j R$, η = the discharge overpotential, R = the resistance per square centimeter of the electrolyte, and j = the current density.

Therefore, CdTe deposition happens at a potential that is more positive than required to deposit Cd as a single phase. This is due to the gain in free energy according to [5] :



If we draw the relation between the current and the voltage, from typical data collected at CSM, we find three regions (see Fig. 2.2):

1. Region i - Only Te can be deposited, and current in this region is proportional to voltage.
2. Region ii - This is the plateau and CdTe can be deposited here. It extends between -0.2 V and -0.625 V vs. Ag/AgCl. The rate of Te deposition is diffusion controlled, so the tellurium current is given by [5]:

$$i_{\text{Te}} = \frac{-4DFC_{\text{HTeO}_2^+}}{\delta} \quad (2.2)$$

where: D = the diffusion coefficient, $C_{\text{HTeO}_2^+}$ = the concentration of HTeO_2^+ , δ = the diffusion layer thickness and F = the Faraday.

The total current will be given by [5]:

$$i_{\text{tot}} = i_{\text{Te}} + i_{\text{CdTe}} = \frac{-6DFC_{\text{HTeO}_2^+}}{\delta} . \quad (2.3)$$

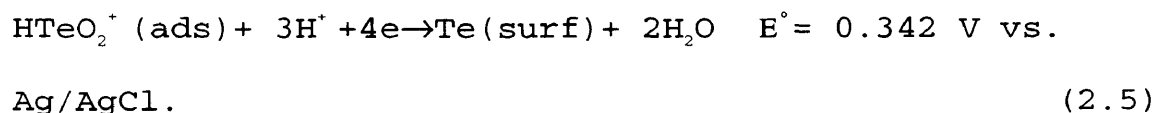
and is proportional to the bulk concentration of Te in region ii.

In this region, the formation of CdTe occurs through a mechanism of reactions. In these steps adsorption takes

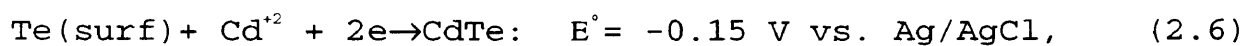
place since Te exists in the bath as the soluble species HTeO_2^+ . So, according to [6]:



Then there is a reduction of the adsorbed species into superficial tellurium according to [7]:



Finally, there is the reduction of superficial tellurium into CdTe [7]:



where E° is the equilibrium potential of the reaction. Fig. 2.3 shows the boundaries for reactions 2.5 (dehydration and discharge) and 2.6 (migration into lattice).

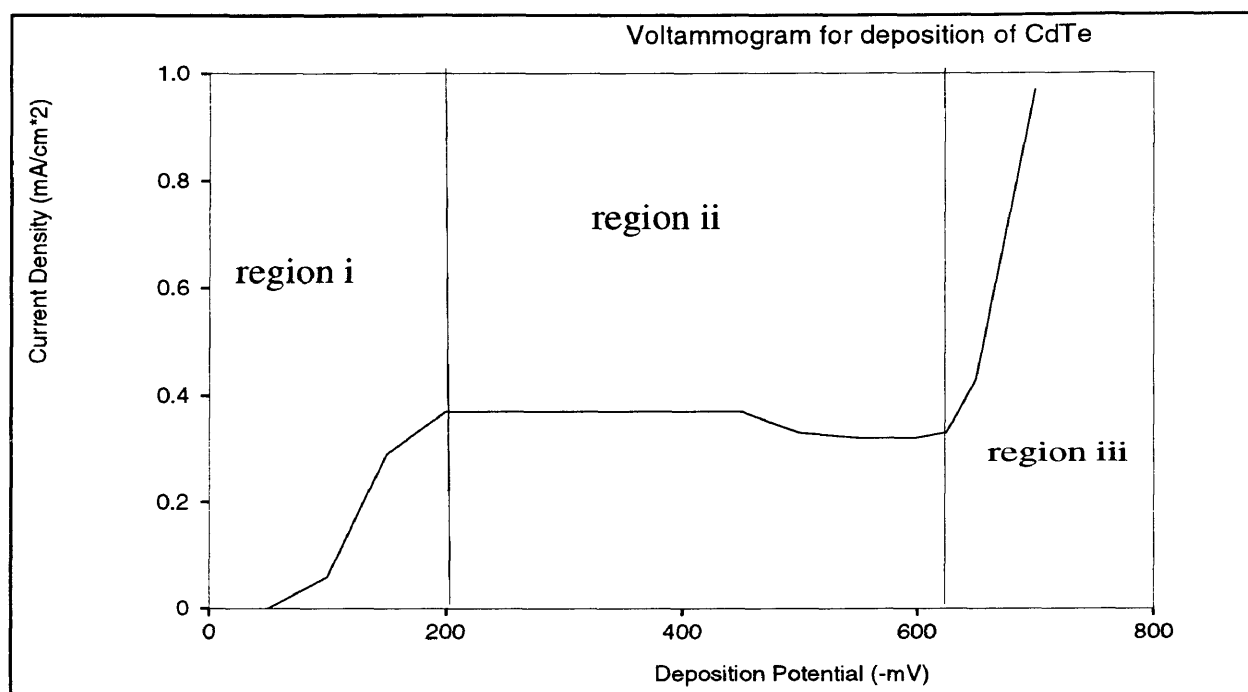


Fig 2.2 Voltammogram for deposition of CdTe

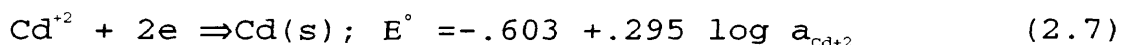
Region ii can be sub-divided into three parts:

a. At relatively positive potentials, CdTe formation doesn't consume all of the Te; reaction (2.1) is faster than reaction (2.5). Therefore, an excess of Te phase is found [5]. Since Cd vacancies and interstitial Te act as acceptors, this will lead to p-type CdTe. Thus, the more positive the deposition potential is, the more Te will be contained, and the higher the acceptor concentration will be.

b. Similarly, the more negative the deposition potential is, the faster will be reaction (2.6). Thus, more Te will be consumed and less free Te will be available which will make the CdTe Cd rich and therefore, n-type.

c. There is a point in between the two regions mentioned above, in which reactions (2.5) and (2.6) are balanced, leading to i-type CdTe (intrinsic CdTe in stoichiometric form). This point is called the potential of perfect stoichiometry(PPS); at this point $a_{\text{Cd}} = a_{\text{Te}}$. The PPS shifts to more positive values as temperature and $a_{\text{Cd}^{+2}}$ are increased [6].

3. Region iii : Here, two reactions are possible: reaction (2.6) and the reduction of cadmium according to[4]:



Reaction (2.7) will be much faster than reaction (2.6), so reaction (2.7) will dominate region iii. As a result, the deposition product in this region will consist mainly of Cd metal.

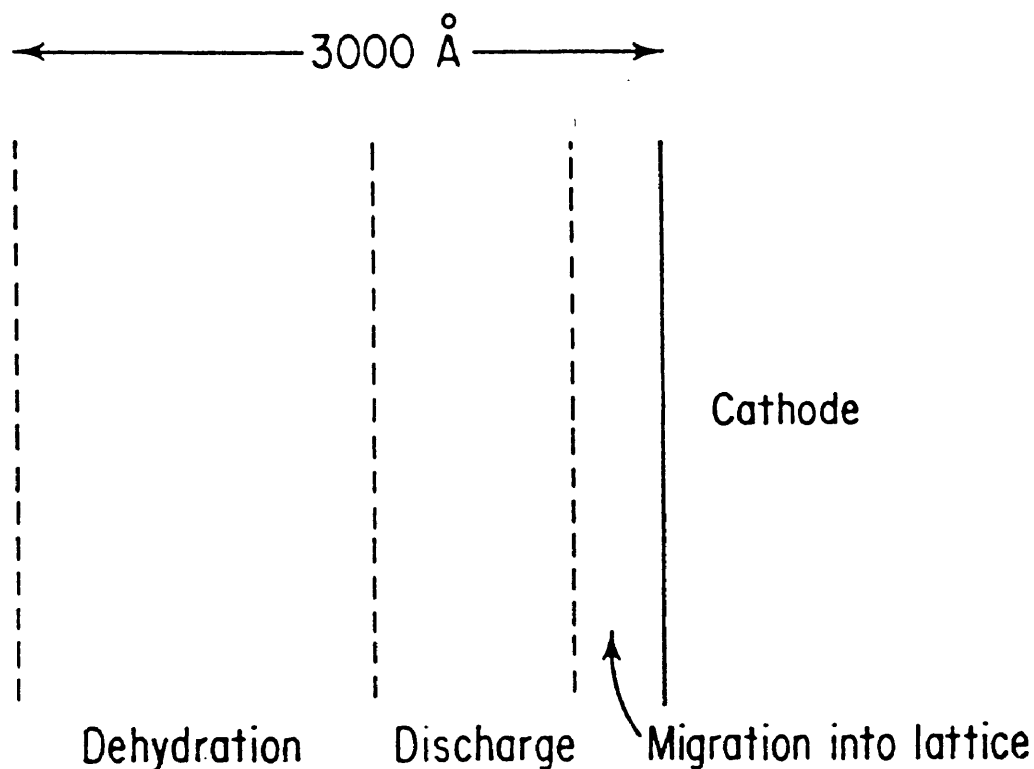


Fig 2.3 Diagram of the reaction regions near the cathode.

2-3. Literature Review of CdTe Electrodeposition

Many groups have studied the cathodic deposition of CdTe from different perspectives. A review of these studies will be presented here, especially those related to change in applied potential.

The Panicker et al. study [4] of cathodic deposition of CdTe is considered as a reference for all those who use electrodeposition as a technique for preparing CdTe (see Fig. 2.4). They used an aqueous solution of CdSO₄ at pH of 2.5-

3. The temperature range was between 25 and 100 °C. They found that films having $0.2 \text{ V} < V_{\text{dep}} < 0.6 \text{ V}$ vs. SCE (saturated calomel electrode) formed CdTe. They also found that the deposit is amorphous at room temperature and semicrystalline with grain size 500-1000 Å when deposited in the range 35-90 °C. Annealing increased the crystalline size to greater than 5000 Å. The CdTe was n-type when deposited at $-V_{\text{dep}} > 0.3 \text{ V}$ vs. SCE, p-type when having $-V_{\text{dep}} < 0.3 \text{ V}$ vs. SCE. The study did not mention either photovoltaic cells or their efficiencies. Also no mention of optical or electrical properties was made.

Takahashi et al. [5] studied the optical and photochemical behavior of CdTe films. Acidic solutions containing CdSO_4 and TeO_2 were used to deposit CdTe. The pH was 1.4 and the depositions were carried out at room temperature. The current-potential relation was very uniform (see Fig. 2.5). They found that CdTe deposited at potentials more positive than -0.4 V vs. Ag/AgCl contained free Te atoms which act as surface recombination centers while films deposited at potentials more negative than -0.4 V were n-type. They also found that the photocurrents of the as grown CdTe films are relatively small. They attributed the major reason for this to the effective recombination of

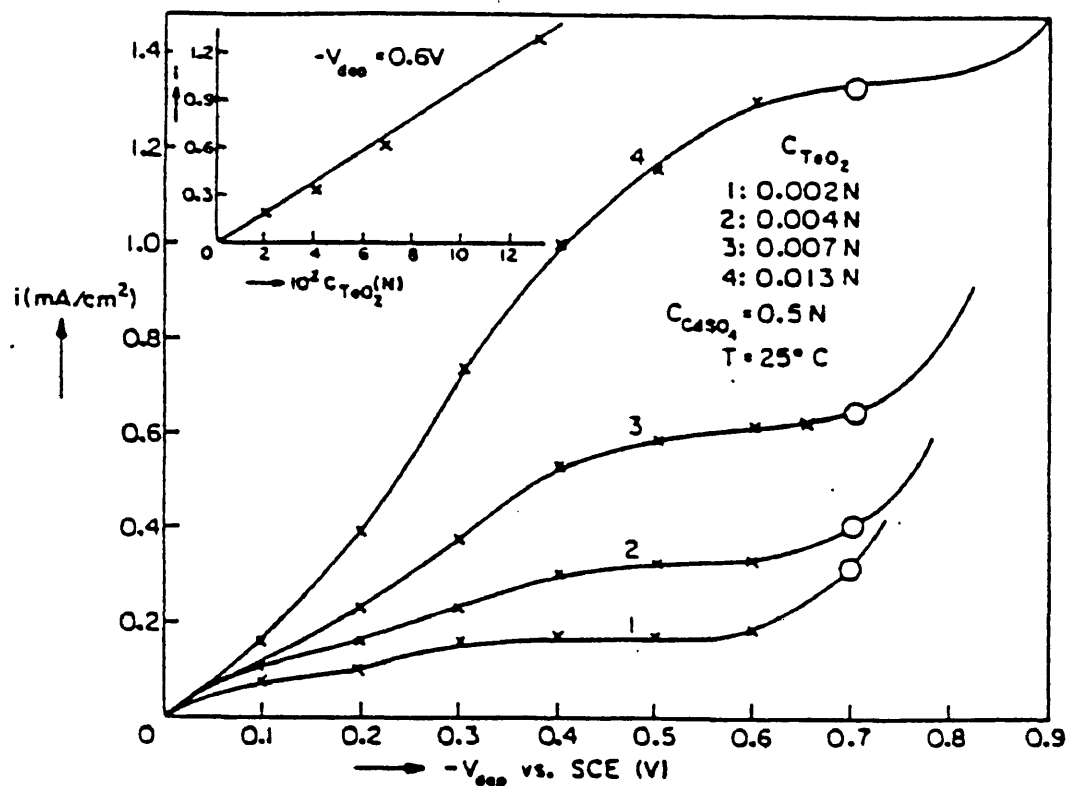


Fig. 2.4 Voltammogram of CdTe from Panicker et al. [4].

electron-hole pairs at grain boundaries and the surface. They noticed that the photocurrent increased significantly after heat treatment. This was attributed to an increase of crystalline diameter and to removal of surface Te which acts as a recombination center.

Sella et al. [7] studied the electrodeposition mechanism of CdTe from acidic aqueous solutions. They found out that the adsorption reaction (see reaction 2.4) plays an important role in the succession of reactions which leads to the

formation of CdTe. The adsorption reaction decreases the deposition rate which leads to a homogeneous deposit.

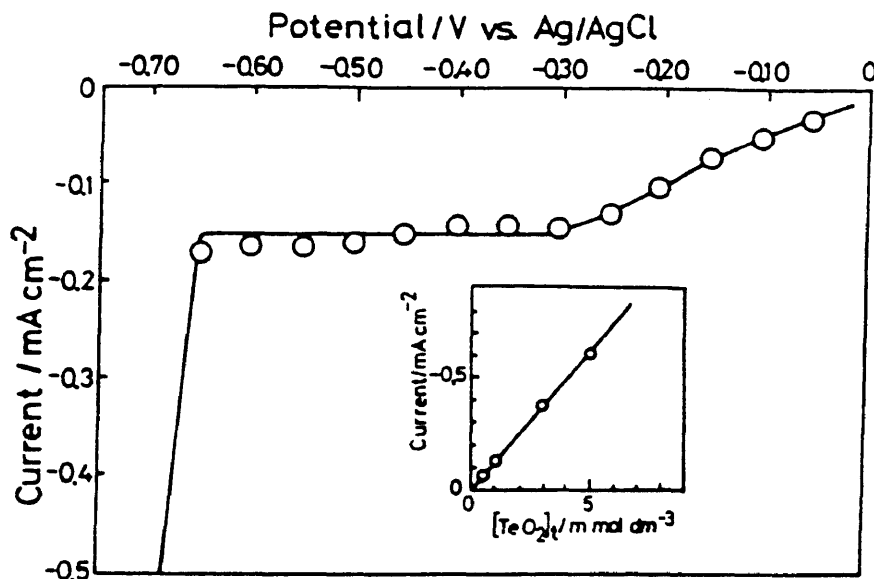


Fig 2.5 Voltammogram of CdTe from Takahashi et al [5].

Kampmann et al. [8] investigated the influence of both the electrodeposition potential in a limited range and the substrate on the properties of CdTe. CdTe layers were characterized by X-ray diffraction, transmission measurements, spectral response, and by scanning electron microscopy. The electrodeposition was carried out in an aqueous solution of sulfuric acid; pH was 2.5, containing 0.8M CdSO₄ and 3x10⁻⁴M HTeO₃⁻. The electrodeposition temperature was 85° C while the electrodeposition potential

was varied in a region of 65 mV. Therefore, two CdTe films were deposited at 5 and 65 mV vs. Cd/Cd²⁺ electrode (the Cd/Cd²⁺ potential lies at about -0.4 V vs. the standard hydrogen electrode, SHE).

The Ametek program in photovoltaics lasted more than ten years before they donated their equipment and know-how to CSM. Ametek was trying to develop procedures for manufacturing polycrystalline thin film solar modules based on CdS/CdTe/ZnTe n-i-p solar cells [9]. The CSM group is pursuing the work of Ametek in both CdTe/CdS and CdTe/CdS/ZnTe structures and has developed devices with a new efficiency record for the deposition technique.

CHAPTER 3

TECHNIQUES

X-ray diffraction (XRD), photoluminescence, Auger spectroscopy and other techniques were used to investigate the characteristics of CdTe samples deposited at different fixed potentials and where the potential was varied during deposition. The microstructure and some optical and electrical properties were studied.

3-1. X-ray Diffraction

X-ray diffraction techniques are described in detail in many books [10]. Only the summaries of the important concepts that were used to analyze the data are described here.

3-1.1. Determination of the Texture

In a polycrystalline material, grains may be randomly oriented or may tend to cluster about some particular orientation; if they do, they are said to have a texture or a preferred orientation. Texture might happen as a result of a forming process and in this case it is called

deformation texture; or it might happen as a result of annealing and in this case it is called recrystallization texture or annealing texture. Preferred orientation is the rule and random orientation is the exception. Thus texture exists in many forms of materials; it exists even in rocks and ceramics.

Texture has a marked effect on the macroscopic properties of materials. An aggregate in a specific direction must have directional properties to some extent. For example, in solar cells it may be important to have preferred orientation along the path of the current.

There are two main types of texture: fiber and sheet texture. Fiber texture is the simpler example. In this type, grains orient themselves parallel to an axis which is called the fiber axis. Materials with this texture have rotational symmetry about the fiber axis. This kind of texture commonly exists in sheets formed by dipping, electroplating, or evaporating. The fiber axis in these materials is perpendicular to the surface and parallel to the columnar crystals. In sheet texture, the grains are in planes roughly parallel to the surface[10].

During the growth of semiconductor thin films, the force of coalescence oriented in a specific direction tries to make the film compact. Thus, most semiconductors have a

preferred growth orientation even on a completely random amorphous substrate[11]. Therefore, cubic materials prefer to grow with the [111] axis normal to the substrate, while hexagonal materials prefer to grow with the [002] axis normal to the substrate[11]. During growth, large aggregates grow at the expense of the small ones forming columnar grains (see Figure 3.1).

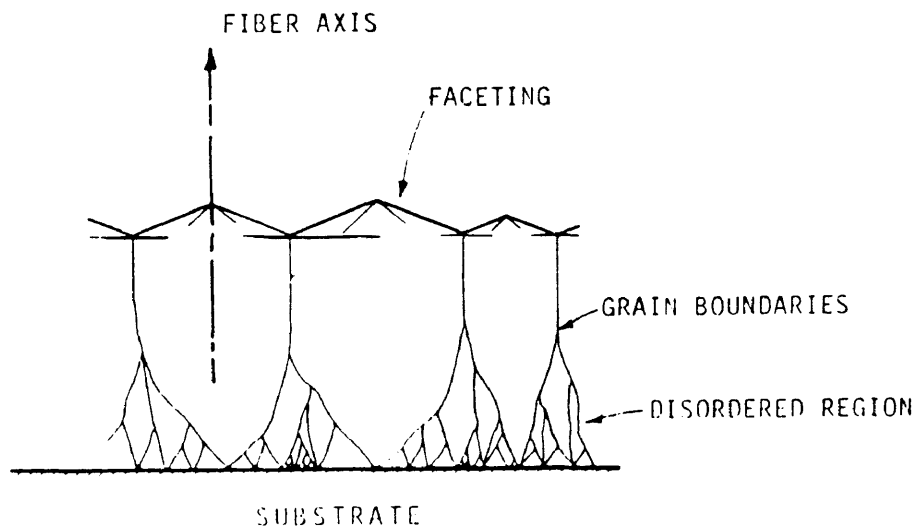


Fig. 3.1 Schematic cross section Of polycrystalline thin film [11]

According to Raub and Muller [12], "H.Ficher, P.Hushe and F.Pawlek found a parallelism between stress, hardness

and texture. They found that maximal tensile stress occurs when the deposits grow according to the field oriented texture type, and maximum compressive stress when growth takes place in accordance with the unoriented type".

In this thesis, the texture of CdTe in both forms, as deposited and annealed, has been studied. Different methods are usually used to find how strongly and in what direction CdTe is textured. These include back reflection, the Laue camera method, comparison with the powder spectrum method, and the diffractometer method. In this study, only the powder spectrum method has been employed. The results might be beneficial to the optimization of CdTe solar cells and their electronic properties.

3-1.2 Calculation of the grain size; the Scherrer Equation

It is desirable that the grain size of the samples prepared be as large as possible to obtain the greatest solar efficiency[11]. The Scherrer equation is often used to calculate the grain size; it utilizes the line broadening of the X-ray spectrum according to:

$$L = \frac{k\lambda}{B \cos \theta} \quad (3.1)$$

where B is the additional breadth of the diffraction line due to finite grain size, measured at half its maximum intensity, λ is the X-ray wavelength, θ is the Bragg angle, L is the mean dimension of the crystallites, and k is a constant approximately equal to unity.

To calculate B , Warren's method is used. In this method, the breadth of the standard peak (powder CdTe) and the breadth of the measured peak are employed to calculate B in the Scherrer equation according to:

$$B^2 = B_m^2 - B_s^2 \quad (3.2)$$

where B_m is the measured breadth and B_s is the standard breadth.

The problem with the Scherrer equation in calculating the grain size is that it ignores other factors like the presence of lattice strains or other imperfections.

3-2. Photoluminescence measurements (PL)

Photoluminescence(PL), meaning luminescence excited by photons, is a tool for investigating both intrinsic electronic transitions and electronic transitions at impurities and defects [13]. This has proven to be a sensitive, nondestructive technique for examining the quality of a material. PL spectra can be used to determine

both the band gap of materials and the stoichiometry of ternary semiconductors. By focusing PL measurements on a spot, they can be used as a sensitive probe of lateral variation in structural quality, impurity concentration, and stoichiometry.

The sample is excited with an optical source, typically a laser with $h\nu > E_g$, generating electron-hole pairs (ehp) that recombine by one of several mechanisms. As mentioned before, photons are emitted by radiative recombination; for nonradiative process the recombination energy is used in the creation of Auger electrons, phonons, and other process which do not result in light emission. For good PL output one would like the majority of the recombination to be radiative.

For radiative recombination, the photon energy depends on the recombination process. There are five commonly observed transitions illustrated in Fig.3.2 [13] :

1.band-to-band: this dominates at room temperature but is rarely observed at low temperature.

2.FE luminescence(free exciton): when the material is highly pure, at low temperatures and at relatively low excitation densities, the excess electrons and holes predominantly form excitons which subsequently decay giving

rise to free-exciton luminescence. The photon energy is less than the band gap energy by the FE binding energy.

3. BE luminescence (bound exciton): if the material contains donors and acceptors with concentrations $> 10^{15}/\text{cm}^3$ and at 4.2 K, virtually all of the free excitons are captured giving rise to bound excitons. BE luminescence lines in this case are sharp and have energies which vary slightly depending upon the particular defect to which the exciton is bound. This includes either a hole combined with a neutral donor or a free electron combined with a neutral acceptor (see fig.2.4). BE recombination dominates over FE recombination for less pure materials.

4. D-A recombination (donor-acceptor): in this case an electron on a neutral donor can recombine with a hole on a neutral acceptor.

5. BMEC luminescence (bound multiexciton): at high excitation densities the donors and acceptors bind more than one exciton.

3-3. Scanning Electron Microscopy (SEM)

SEM is a powerful technique for exploring the structure of the samples at magnifications as high as 20,000. Descriptions of this technique are available in many books [14].

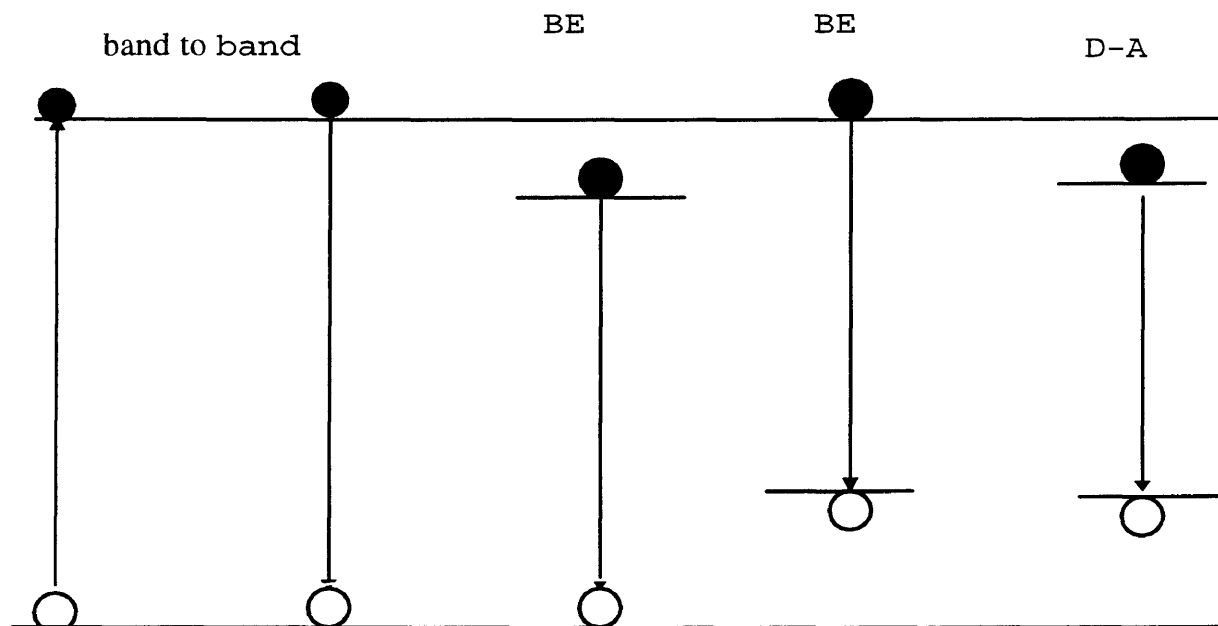


Fig. 3.2 Radiative transitions observed with PL.

3-4. Auger electron spectroscopy (AES)

This is a technique used to identify the elemental composition and sometimes even the chemical bonding of the atoms in the surface of samples. By using Auger in combination with sputtering, it is possible to obtain elemental composition as a function of depth. Detailed information about its principles and applications can be found in many references [15].

3-5. Hot Probe

This technique is used to determine whether a semiconductor is n-type or p-type. This was necessary in the present case to find out the point of perfect stoichiometry (PPS). The set up simply consists of a hot point probe, a cold point probe and a voltmeter. The hot point probe measurements were conducted using copper wire wound around a soldering iron gun, while the cold point probe was the hand held multimeter probe. (See fig. 3.3.)

To do the measurement, the hot probe is allowed to heat up and then both probes are brought into contact with the semiconductor sample. The sign of the voltage will indicate the semiconductor type. The space between the probes can be reduced to enhance the voltage.

In the vicinity of the probe contact, the heated probe creates an increased number of higher energy carriers. These carriers will be holes in the case of p-type material and electrons in the case of n-type material. Then, these energetic carriers diffuse away from the hot probe through the semiconductor sample. The result is a deficit of holes or a net negative charge in the vicinity of the hot probe for p-type material and a deficit of electrons or a net positive charge in the vicinity of the hot probe for n-type material. So, the type is determined by the sign of the

thermal emf or Seebeck voltage generated by the temperature gradient. These thermal gradients produce an electric field in a semiconductor. The electric field for n or p-type materials is given by:

$$\vec{E} = S \vec{\nabla} T \quad (3.3)$$

$$\Delta V = -\int \vec{E} \cdot d\vec{l} = -S \int \vec{\nabla} T \cdot d\vec{l} \quad (3.4)$$

where S is the Seebeck coefficient.

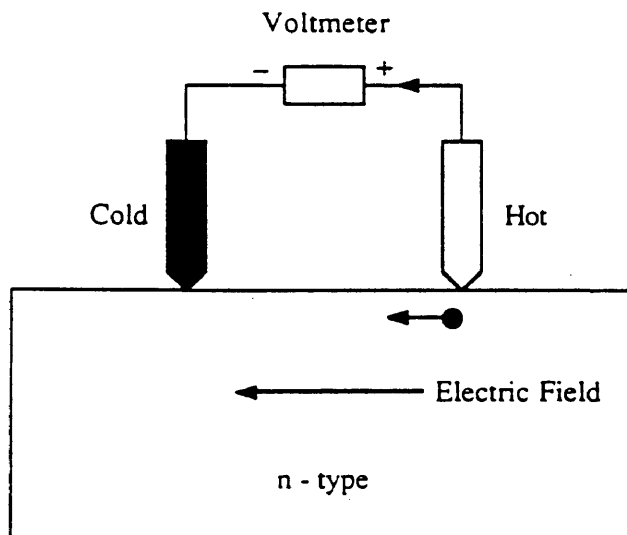


Fig. 3.3 Schematic diagram of the hot probe set up.

CHAPTER 4
EXPERIMENTAL DETAILS

4-1. Sample Preparation

Samples were prepared by the electrodeposition technique on glass/SnO₂/CdS. Contacts were made to the CdS surface using indium solder. Then, bare ends of teflon insulated copper wires were attached to each of the indium strips and the bare metal was sealed with an electrically insulating coating. Then the sample was fixed at the cathode at the electrodeposition system and the CdTe was deposited as described in chapter 2. The thickness of the CdTe was about 2 μm. The deposition potential of the different samples is given by Table 4.1 and details of the variable potential sample are shown in Table 4.2.

Table 4.1 Deposition Potentials of CdTe samples

Sample	Deposition Potential(-mV)
46-5	400
46-3	500
46-6	600
82-2	variable potential

Table 4.2 Variable potential deposition data (sample 82-2)

Deposition Potential (mV)	Time (Minutes)
-400	15
-500	40
-550	40
-600	40

All samples were treated with CdCl_2 and annealed under 410 C° in air for 45 minutes (see [16] for a description of the annealing process).

4-2. X-ray Diffraction (XRD)

A Rigaku X-ray diffractometer using Cu as a target was used to perform the XRD measurements. The texture was determined using relative integrated intensity, while the full width at half maximum was used to determine the grain size using the Scherrer method [10]. The scanning range for 2θ was from 10° to 90° which contains many of the major peaks of CdTe. The scanning step size was $0.05^\circ 2\theta$ and the time interval was two seconds per step.

4-3. Auger electron spectroscopy (AES)

Auger electron spectroscopy (AES) can be used to study the elemental components in a few atomic layers at the surface. However, when AES is used along with ion-sputtering removal of the atomic layers to obtain a compositional depth profile below the surface, it can be a much more powerful tool. Ion-sputtering removal can be done simultaneously with the compositional analysis.

4-3.1 Depth Profiling by Ion Sputtering

Ion-sputtering is a powerful tool for depth profile analysis. However, it has some disadvantages. The nonuniform erosion of ion sputtered surfaces has been the subject of many studies [17]. Sometimes conical structures are obtained in the sputtered crater after ion sputtering. These are thought to be a result of sputter resistance apexes in the sample [17]. Instrumental effects can also contribute to a loss of depth resolution because of uneven current distribution over the sputtered area.

Two factors affect the depth profile resolution between two materials: the removal of atoms by the ion sputtering process and the roughness of the interface referred to the initial roughness of the sample surface. The depth resolution is measured by the interface depth broadening.

According to Lea and Seah: "The interface broadening

due to the sputtering process has three major contributions: the statistics of sputtering, the roughness of the surface and knock-on damage" [17].

Studies show that the broadening of the interface in the compositional depth profiles is a function of the film thickness and surface roughness. For rougher surfaces, a clear degradation of depth resolution was observed. Fig.4.1 shows the deterioration of the resolution as the ion beam moves away from normal incidence for several values of θ .

4-3.2. Depth Profiling By Mechanical Polishing

To avoid the disadvantages of ion-sputtering depth profiling, to save time, and to keep the machine free of contamination, attempts have been made to mechanically polish the samples at a very shallow angle. Additionally the sample is scanned laterally with the electron probe for Auger electron analysis as shown in Figure 4.2. The angle-polished region exposes the entire depth to be profiled and analyzed.

Mechanical polishing was done with the use of an Al_2O_3 polishing powder in a few drops of water and fixing the sample in a special tool which allows the sample to be held at a shallow angle relative to the polishing surface. After

the polishing the samples were rinsed using methanol to remove the polishing remnants.

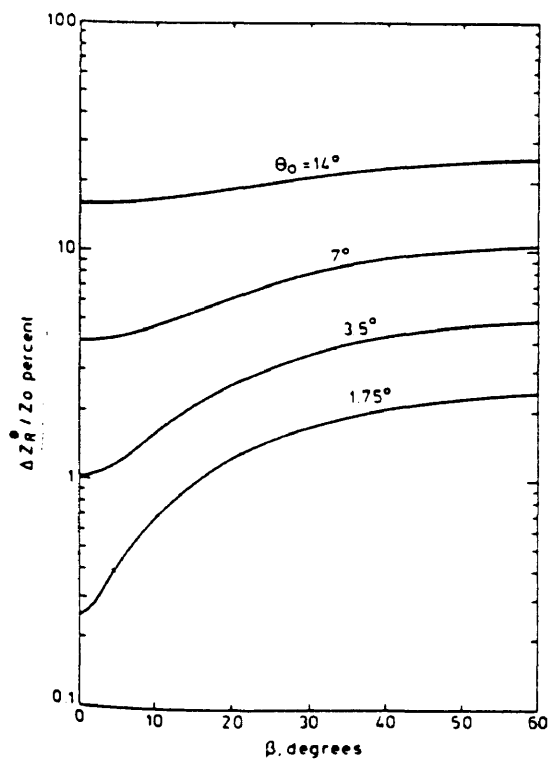


Fig.4.1 The depth resolution for films evaporated along the surface normal for rough substrate subsequently sputtered with ions at an angle β from the surface normal [17].

The use of the mechanically polished depth profile technique has many advantages over the ion-sputtered depth profiling method. These advantages appear when analyzing

samples with initially unknown trace impurities or with samples for which the region of interest is very thin and may be missed by ion sputtering. Besides, mechanically polished samples have the advantage of optimum use of machine time by allowing the interface to be located before taking a lot of measurements which permits a high density data to be recorded near the interface and low density in the constant composition regions. Furthermore, the use of mechanically polished samples will expose the instrument to minimum contamination. According to Lea and Seah. "A final advantage is the availability of a direct precise measurement of the depth scale"[17].

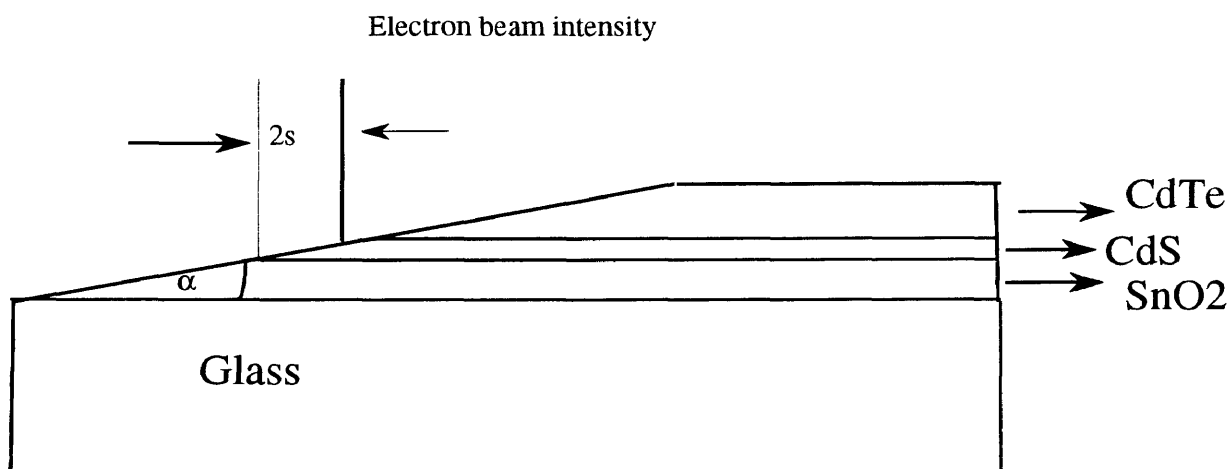
The information is received from a depth

$$Z = x \tan \alpha \quad (4.1)$$

with a resolution in depth due to finite width of beam of:

$$\Delta z_{\alpha} = 2s \tan \alpha \quad (4.2)$$

where $2s$ is the electron beam Gaussian diameter and α is the lapper taper angle. The lapping angle in our study was about 0.4° .



Cross section of mechanically polished sample

Fig. 4.2

4-4. Photoluminescence(PL)

According to Abou-Elfotouh and Coutts [18] the determination of the origin of the defect levels in CdTe films is based on the change in both the PL peak position and intensity with measuring temperature and excitation power. In this work, the PL measurements were taken for the as-deposited samples at low temperature (9K) to find the defect levels in these samples in that state. For the annealed samples, PL measurements were taken at room temperature to find the band gap of these samples and also at low temperature (5K) to find how the defect levels changed after annealing.

The PL arrangement (see Figure 4.3) consisted of the source which was a laser with a certain excitation energy, a cryostat which was used to cool down the sample, a double-grating monochromator, and a photomultiplier tube which was used to detect the signal. The resolution of the system was determined by the focal length of the monochromator, slit width, and the grating spacing. For a better signal-to-noise ratio, the detector was cooled. The sample in the cryostat also was cooled to produce sharper, more readily identifiable peaks. Cooling the sample also tends to reduce the role of competing nonradiative paths for recombination, giving rise to an improved signal-to-noise ratio. Finally cooling prevents impurity centers from undergoing thermal ionization.

4-5. Efficiency Measurements

The setup consists of a personal computer, software, input-output hardware, and an ELH projector lamp. The measurement is done by mounting a cell onto a special holder and exposing it to the ELH lamp. The ELH lamp gives illumination close to 1.5 AM illumination and is calibrated with a standard GaAs cell. Leads were connected from the holder to input-output hardware, connected to a personal

computer. Measurements were recorded automatically by the pc.

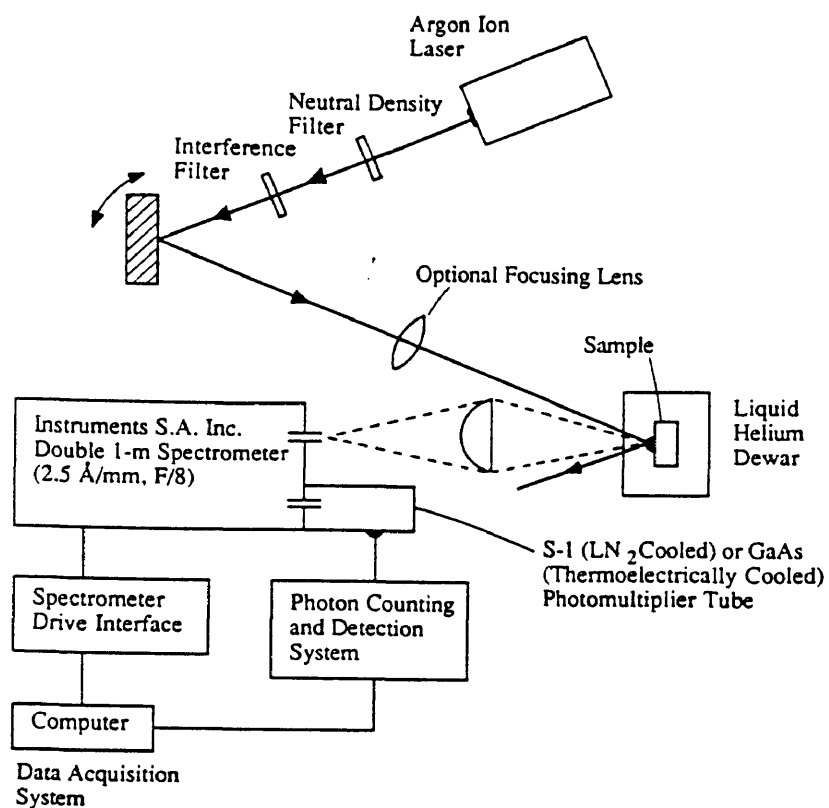


Fig. 4.3 A typical apparatus used for photoluminescence measurements [14].

CHAPTER 5
RESULTS AND DISCUSSION

5-1 Hot probe measurements

This technique showed that samples prepared at a deposition potential which is more positive than -400 mV are p-type in the as-deposited case, while samples prepared at potentials equal to or more negative than -400 mV are n-type in the as-deposited form. After annealing, all samples are p-type.

5-2 X-Ray Diffraction

5-2.1 Texture

According to Siegfried Mader " preferred orientations are indicated if the ratios of integrated intensities of several reflections deviate from the ratios found in randomly oriented powder specimen" [19]. Therefore the XRD pattern of very fine powder CdTe was calculated and measured.

Given the formulas: $I = F^2 p \left\{ \frac{1 + \cos^2(2\theta)}{\sin^2(\theta) \cos(\theta)} \right\}$ (approximate) and

$$|F|^2 = 16(f_{cd}^2 + f_{te}^2) \quad \text{if } (h+k+l) \text{ is odd}$$

$$|F|^2 = 16(f_{\text{Cd}} - f_{\text{Te}})^2 \quad \text{if } (h+k+l) \text{ is an odd multiple of } 2$$

$$|F|^2 = 16(f_{\text{Cd}} + f_{\text{Te}})^2 \quad \text{if } (h+k+l) \text{ is an even multiple of } 2 \quad [10]$$

and the tabulated key parameters in Table 5.1, the integrated peak intensities can be calculated. They are shown in Table 5.1. The h , k and l are Miller indices, θ is the Bragg angle, λ is the x-ray wavelength, F is the structure factor, f_{Cd} and f_{Te} are atomic scattering factors for Cd and Te respectively (appendix 12 in [10]), P is the multiplicity factor and I is the relative integrated intensity (arbitrary units). The measured XRD of powder CdTe is shown in Table 5.2 and in Figure 5.1.

Table 5.1 Calculation of integrated intensities of powder CdTe

line	hkl	θ	F^2	P	$\frac{1+\cos^2(2\theta)}{\sin^2(\theta)\cos(\theta)}$	I	normalized intensity
1	111	11.86	62708	8	44.16	22544780	1.0
2	220	19.62	$1.18 \cdot 10^5$	12	15.10	21492378	0.95
3	311	23.19	38160	24	10.35	9478944	0.42
4	400	28.36	69696	6	6.53	2718144	0.12
5	331	31.17	28928	24	5.29	3700469.8	0.16
6	420	32.08	256	24	4.97	30535.68	0.001
7	422	35.57	57700	24	4.006	5547000	.25

Table 5.2 Measured integrated intensities of powder CdTe

line	hkl	θ	height	integrated intensity	normalized intensity
1	111	11.8	4453	1048	1.00
2	220	19.58	5129	1150	1.10
3	311	23.14	2461	659	0.63
4	400	28.32	509	165	0.16
5	331	31.13	1090	270	0.26
6	422	35.5	1021	262	0.25

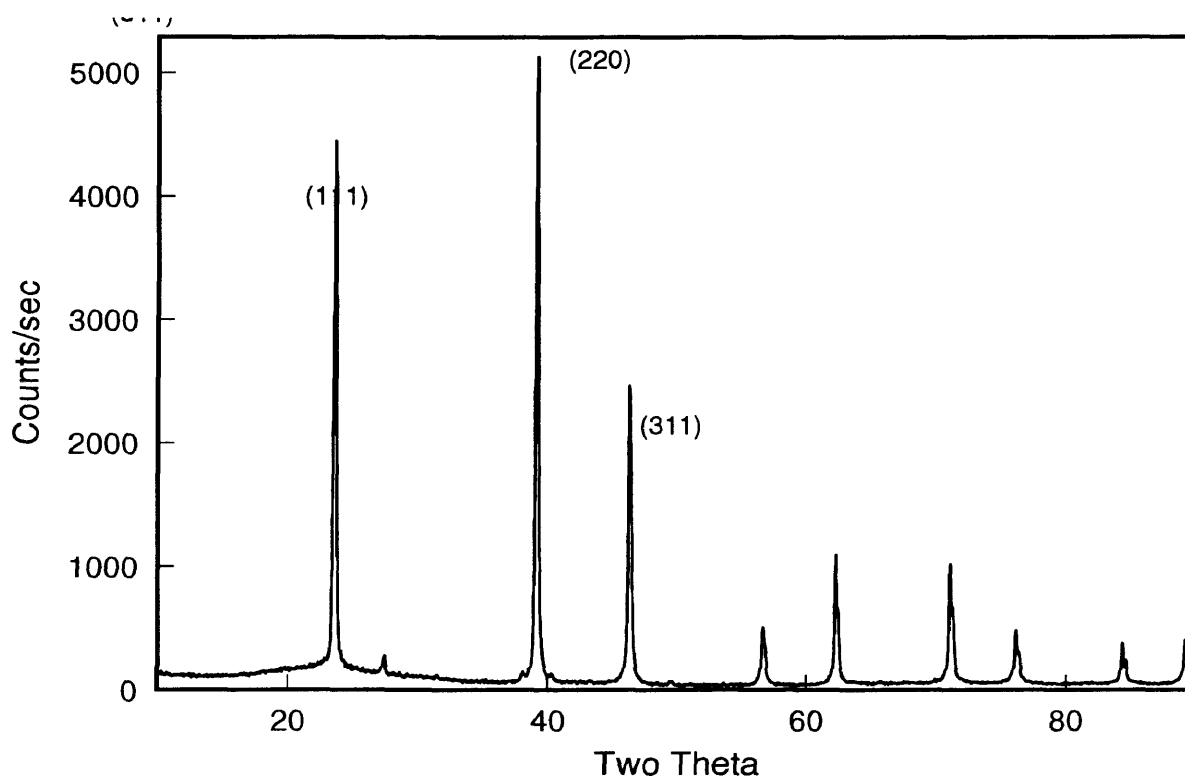


Fig.5.1 XRD pattern of powder CdTe

Now, compare these values with the values obtained for the sample(46-6) in the as deposited state as shown in Figure 5.2 and Table 5.3. It is clear that the [111] direction dominates the pattern of the as deposited CdTe as expected for thin films of cubic materials. The (220) and (311) peaks appear in the as-deposited sample but they are very weak compared to those of the powder (about .5%). The rest of the peaks do not appear in the XRD pattern of the as-deposited CdTe.

Table 5.3 Integrated intensities of as grown CdTe 46-6

line	hkl	θ	height	integrated intensity	normalized intensity
1	111	11.85	11714	5564	1
2	220	19.67	176	26	0.005
3	311	23.32	187	20	.004
4	400	28.32	0	0	0
5	331	31.1	0	0	0
6	422	35.5	0	0	0

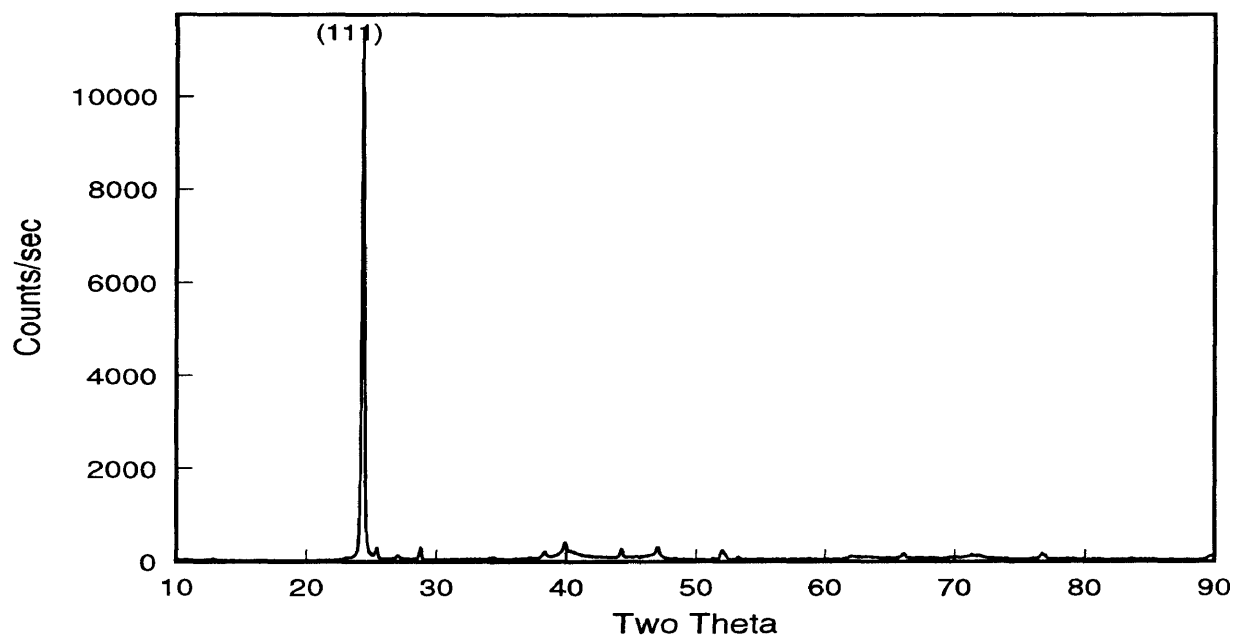


Fig. 5-2 XRD pattern of as deposited CdTe (sample 46-6)

The results for the annealed state are presented in Figure 5.3 and Table 5.4. After annealing, recrystallization occurs and modifies the texture of the as-deposited sample. Most of the peaks in the powder form appear in the annealed CdTe with different integrated intensities as follows:

(111): This peak is still strong in the annealed CdTe but not the strongest.

(220): This is the dominant peak in this annealed form. It is about three times stronger than the same peak in the powder form and about six hundred times stronger than the same peak in the as-deposited form.

(311): This peak is strengthened also by the annealing process. It is about two hundred times stronger than the same peak in the as-deposited form and about two times the same peak in the powder form.

(400) (331) and (422) peaks: These peaks do not show up in the as-deposited form, so they are a result of the recrystallization process. Comparing the integrated intensities of the peaks gives the following results: the (400) peak has the same strength as that in the powder form; the (331) peak is about two times stronger than the same peak in the powder form; and the (422) peak is about the same strength as the same peak in the powder form.

Table 5.4 XRD pattern of annealed CdTe (sample 46-6)

line	hkl	θ	height	integrated intensity	normalized intensity
1	111	11.87	5972	1581	1
2	220	19.66	15826	4688	3
3	311	23.24	3456	1101	0.7
4	400	28.42	442	179	0.1
5	331	31.27	1483	653	0.4
6	422	35.67	869	307	0.2

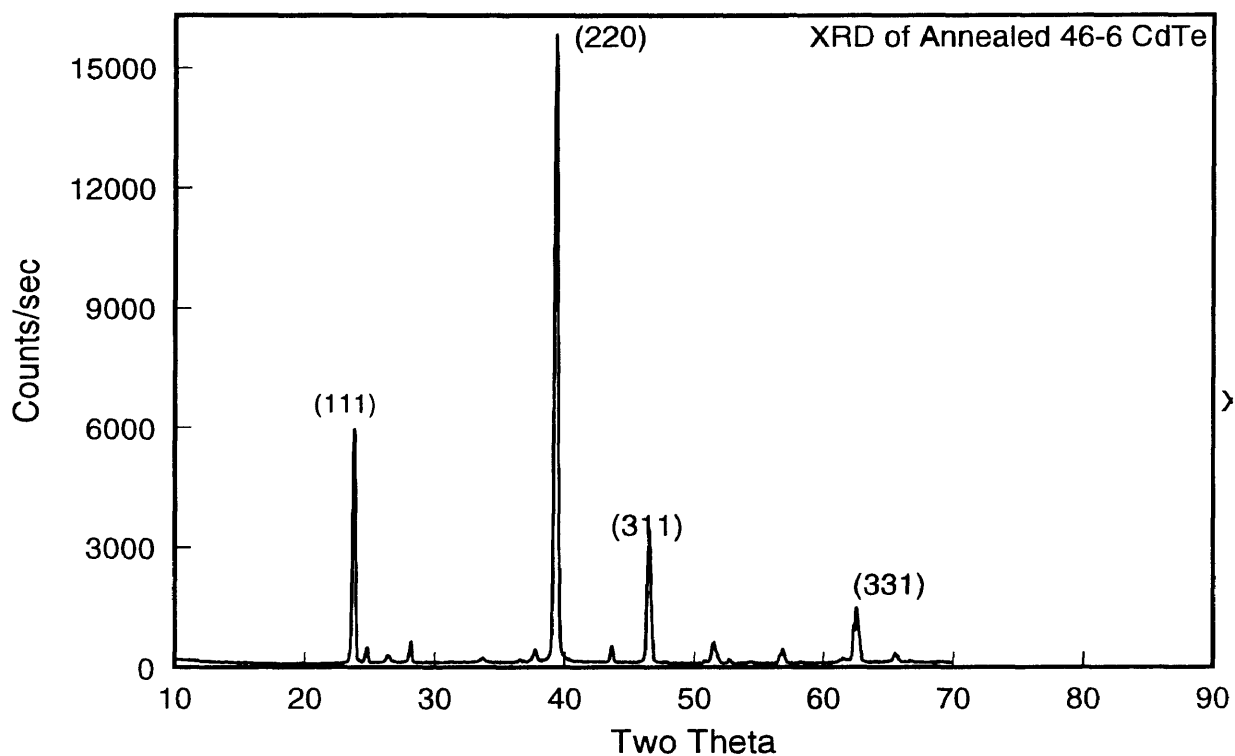


Fig. 5.3 XRD of Annealed CdTe (sample 46-6)

For sample 46-5 in the as-deposited state, the results are shown in Figure 5.4 and in Table 5.5. As in the case of sample 46-6, in sample 46-5 the (111) peak is dominant. However other peaks exist as well although they are very weak. In particular, peaks (220), (311) and (422) show up in the as-deposited case.

The results for sample 46-5 in the annealed state are as presented in Fig. 5.5 and in Table 5.6. After annealing more peaks appear with (111) being the dominant peak. The texture of this sample after annealing looks very similar to the texture of powder CdTe with no preferred orientation.

Table 5.5 XRD pattern of as-deposited CdTe sample 46-5

line	hkl	θ	height	integrated intensity	normalized intensity
1	111	11.9	46500	13907	1
2	220	19.65	725	353	0.03
3	311	23.2	537	260	0.02
4	400	-	-	-	-
5	331	31.2	327	124	0.01
6	422	35.4	416	277	0.02

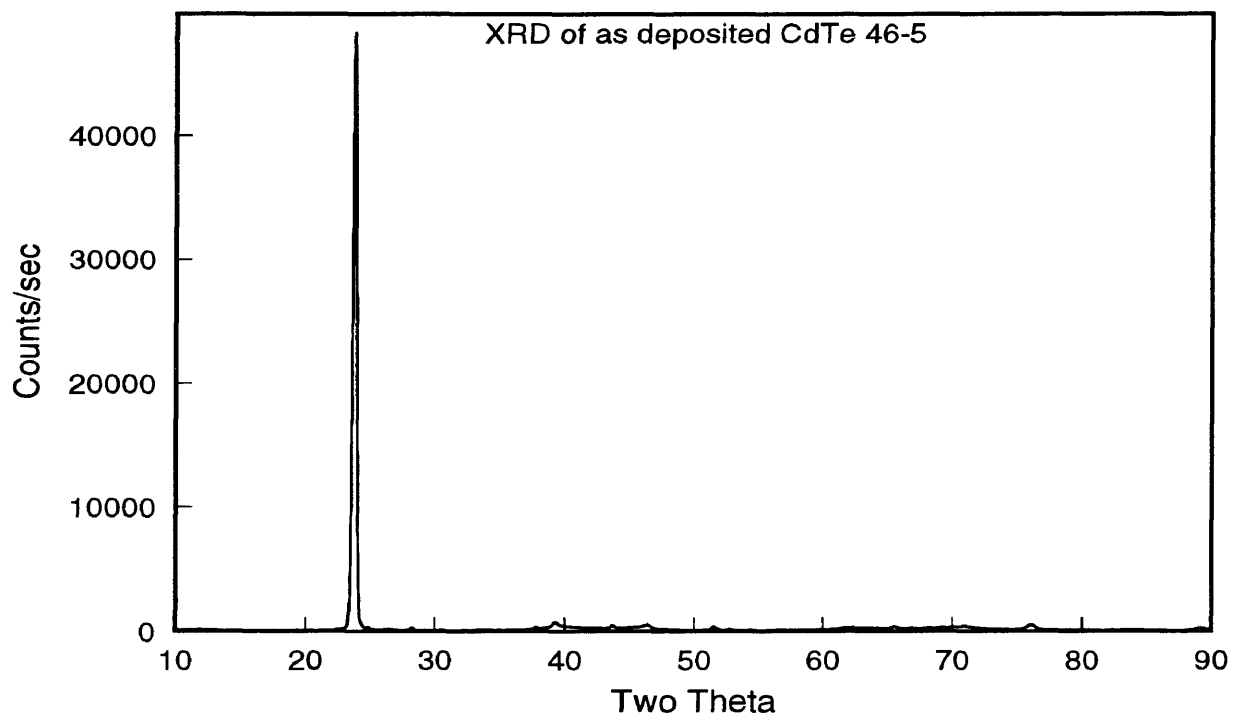


Fig. 5.4 XRD pattern of as-deposited CdTe 46-5.

Table 5.6 XRD pattern of annealed 46-5.

line	hkl	θ	height	integrated intensity	normalized intensity
1	111	12.05	14214	2899	1
2	220	19.78	11056	2627	0.91
3	311	23.2	2478	601	0.21
4	400	28.36	557	170	0.06
5	331	31.15	1409	448	0.15
6	422	35.57	915	342	0.12

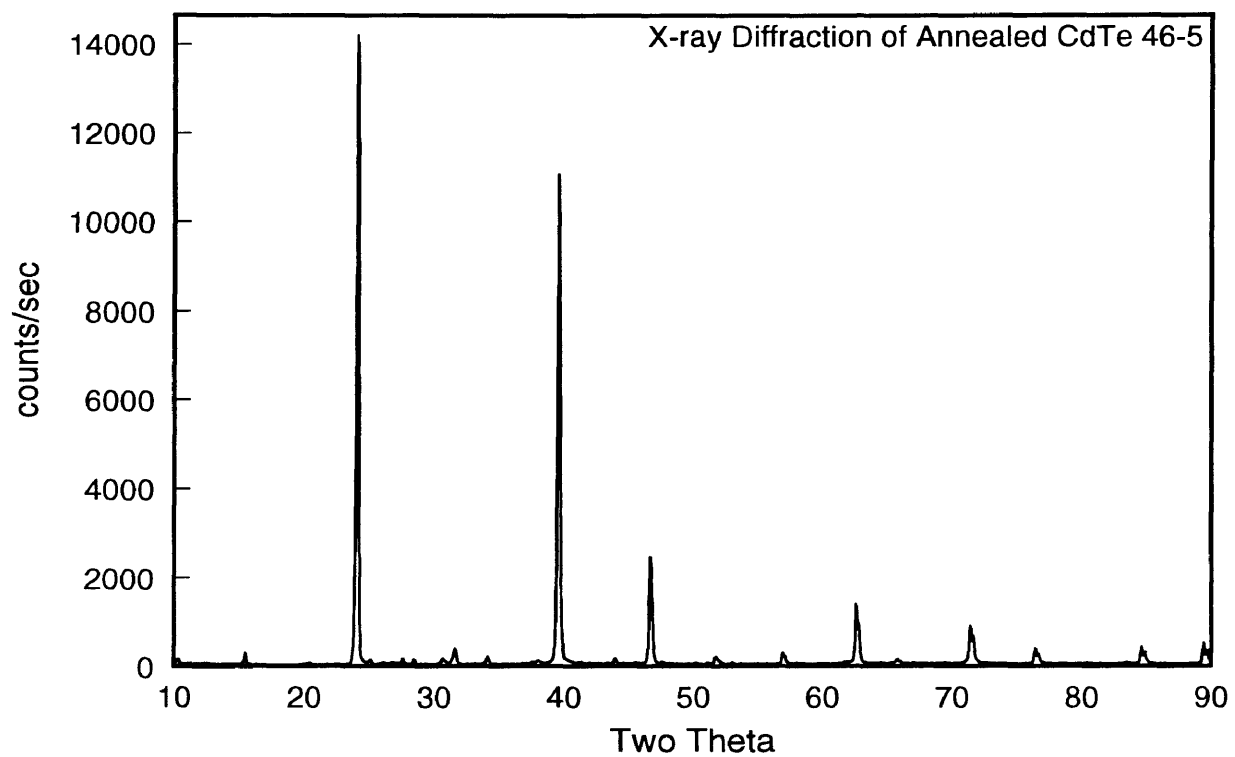


Fig. 5.5 XRD pattern of annealed CdTe (sample 46-5).

For sample 46-3 in the as deposited case, the results are in Figure 5.6 and in Table 5.7. More peaks appear in the as-deposited case than for sample 46-6 but less than for sample 46-5. However, the (111) peak is still the dominant peak while the rest of the peaks are weaker than the similar peaks in sample 46-5. The sample is strongly textured in the (111) direction.

The results for sample 46-3 in the annealed state are presented in Fig. 5.7 and in Table 5.8. After annealing, (220) becomes the dominant peak which is two times stronger than the (111) peak. It is also two times stronger than the same peak in the powder form. The (311) peak is also strong; it becomes stronger than the same peak in the powder form. In addition, the (400), (331), and (422) peaks exist with (422) been the strongest among them.

For the variable potential sample 82-2 in the as-deposited case, the results as shown in Figure 5.8 and in Table 5.9. As in all other CdTe samples, in this sample the [111] direction dominates in the as-deposited case. This sample is strongly textured in the [111] direction. The other peaks, namely (220), (311) and (422) appear with similar strength but they are weak compared with the (111) peak.

Table 5.7 XRD pattern of as-deposited 46-3.

line	hkl	θ	height	integrated intensity	normalized intensity
1	111	12	84000	15347	1
2	220	19.75	379	123	0.01
3	311	23.25	279	107	0.01
4	400	-	NA	-	-
5	331	-	NA	-	-
6	422	35.52	339	114	0.01

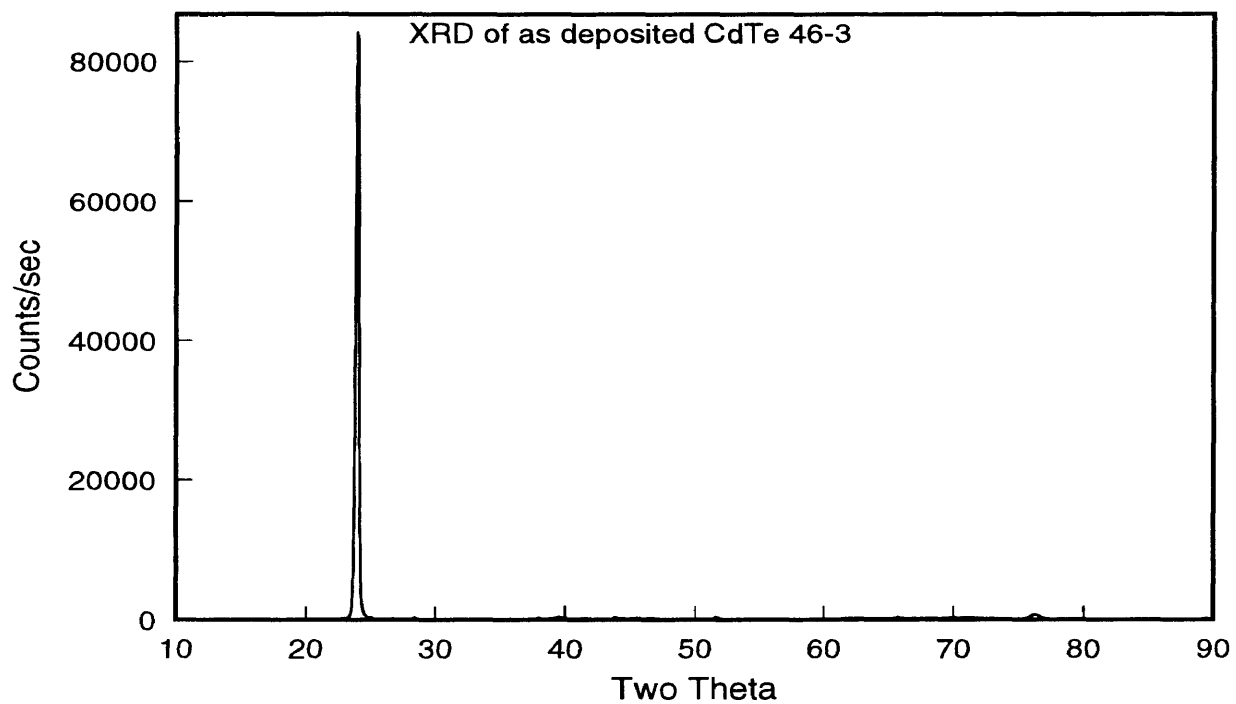


Fig. 5.6 XRD pattern of as-grown CdTe (sample 46-3).

Table 5.8 XRD pattern of annealed CdTe (sample 46-3).

line	hkl	θ	height	integrated intensity	normalized intensity
1	111	11.89	8132	1943	1
2	220	19.65	15625	3779	2
3	311	23.22	2589	628	0.32
4	400	28.35	346	112	0.06
5	331	31.2	1859	585	0.30
6	422	35.58	1070	379	0.19

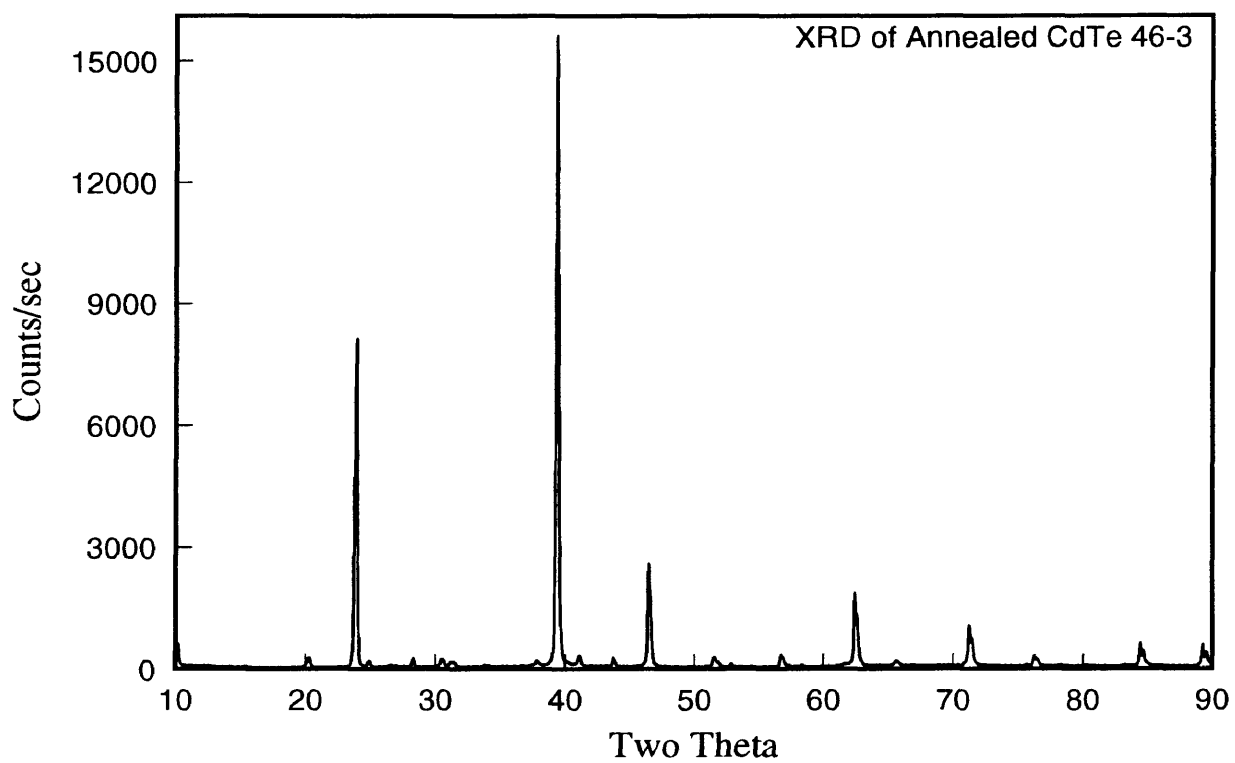


Fig. 5.7 XRD pattern of annealed CdTe (sample 46-3).

Finally, for the annealed state of sample 82-2 the results are shown in Figure 5.9 and in Table 5.10. After annealing, (220) becomes the dominant peak which is four times stronger than the (111) peak. It is also five times stronger than the same peak in the powder form. The (311) peak is also strong; it becomes about two times stronger the same peak in the powder form. In addition, (400), (331), and (422) exist with (331) being the strongest among them.

Table 5.9 XRD pattern of as-grown CdTe (sample 82-2).

line	hkl	θ	height	integrated intensity	normalized intensity
1	111	12.05	82000	13328	1.00
2	220	19.82	254	84	0.006
3	311	23.37	220	56	0.004
4	400	NA	NA	-	-
5	331	NA	NA	-	-
6	422	35.525	339	114	0.009

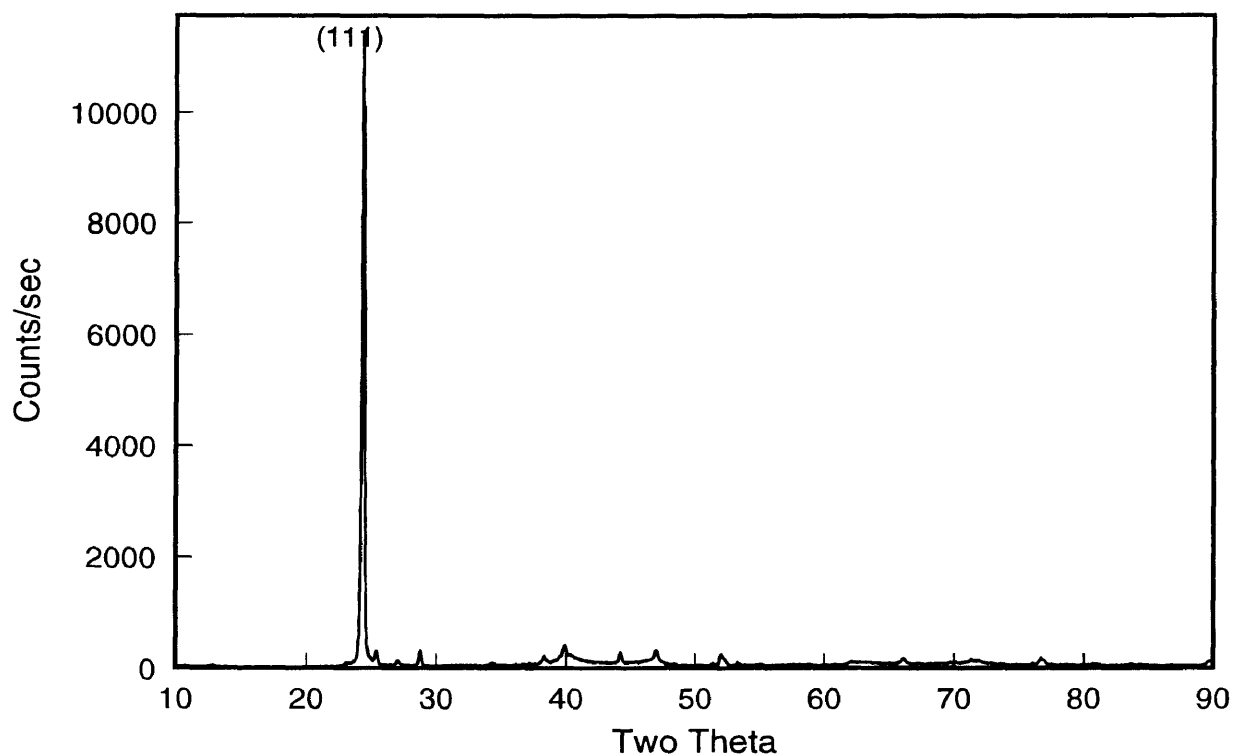


Fig. 5.8 XRD pattern of as-grown CdTe (sample 82-2).

Table 5.10 XRD pattern of annealed CdTe (sample 82-2).

line	hkl	θ	height	integrated intensity	normalized intensity
1	111	12.02	5100	1040	1
2	220	19.78	19665	4467	4.3
3	311	23.34	3838	892	0.85
4	400	28.48	240	70	0.07
5	331	31.31	2066	492	0.47
6	422	35.7	1119	254	0.24

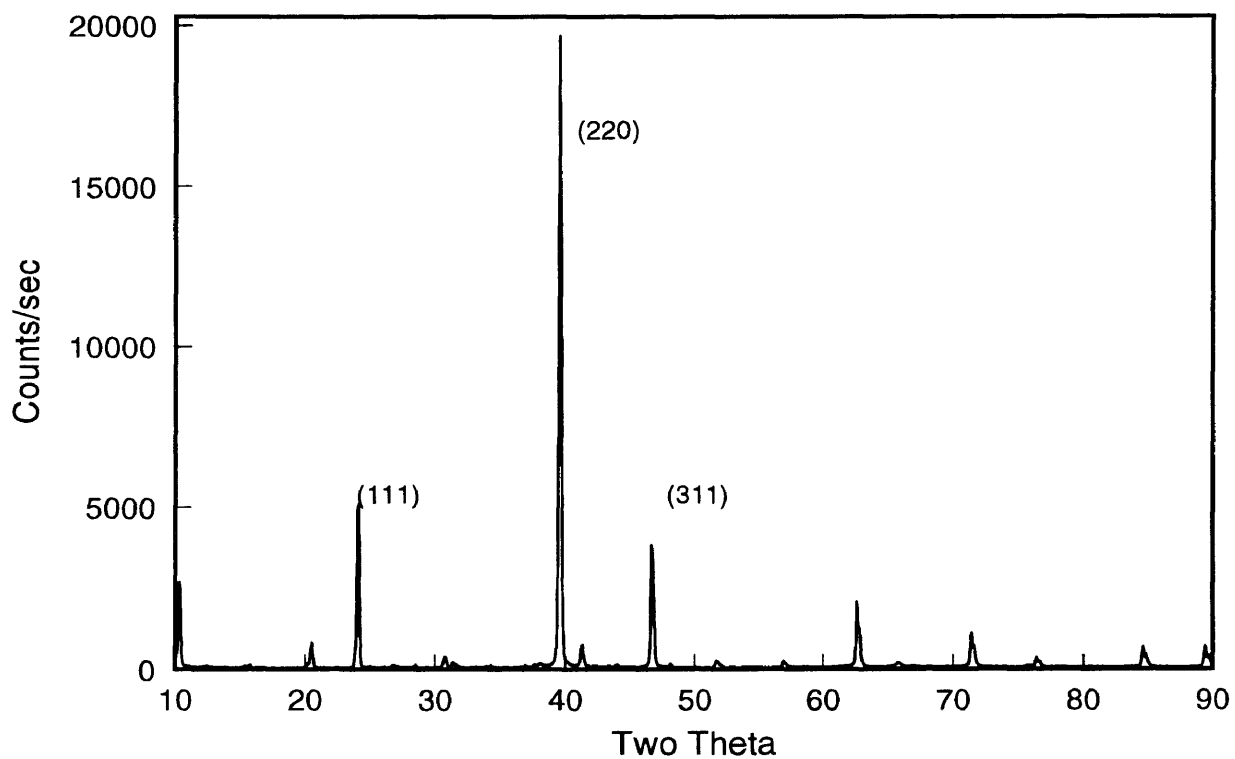


Fig. 5.9 XRD pattern of annealed CdTe (sample 82-2).

5-2.2 Grain Size

Grain size plays a major role in the electrical and optical characteristics of thin films [11]. Tables 5.11 and 5.12 below show the average grain sizes of the as-deposited and annealed samples. It is clear that grain size is influenced by the deposition potential of the samples as well as the annealing.

5-3 Scanning Electron Microscopy (SEM)

SEM Images of the samples 46-5, 46-3 and 82-2 are shown in Figures 5.10, 5.11, and 5.12 respectively. It is clear from the images that the variable deposition potential sample has a much larger grain size than the other samples. This apparently enhances its performance significantly. Its grain size is also uniform throughout the sample. The grain sizes of the fixed potential samples are not uniform and cover a wide ranges. Table 5.13 below, from SEM measurements, shows the maximum grain sizes for the fixed potential samples and the uniform grain size for the variable potential sample. These maximum grain sizes are clearly much larger than the average grain size estimated by XRD as given in Tables 5.11 and 5.12.

Table 5.11 Calculated grain sizes of annealed CdTe.

sample	hkl	B_M	B	B(radian)	θ	grain size(\AA)
46-5	111	0.223	0.058	0.00101	11.87	1400
	220	0.268	0.142	0.00247	19.63	600
	311	0.291	0.107	0.00187	23.2	810
46-3	111	0.295	0.202	0.00353	11.89	400
	220	0.304	0.201	0.00351	19.65	420
	311	0.321	0.172	0.00300	23.22	500
46-6	111	0.234	0.091	0.00158	11.87	900
	220	0.273	0.151	0.00264	19.86	560
	311	0.303	0.136	0.00238	23.23	640

Table 5.12 Calculated Grain sizes of as-deposited CdTe.

sample	hkl	B_M	B	B(radians)	θ (degrees)	grain size(\AA)
46-5	111	0.333	0.2543	0.00443	11.87	310
46-3	111	0.262	0.1494	0.0026	11.89	520
46-6	111	0.229	0.0797	0.00139	11.87	980

Table 5.13 Grain size for annealed CdTe.

Sample	Grain size (μm)
82-2	1.5-2
46-5	0.3
46-3	0.35
46-6	0.275

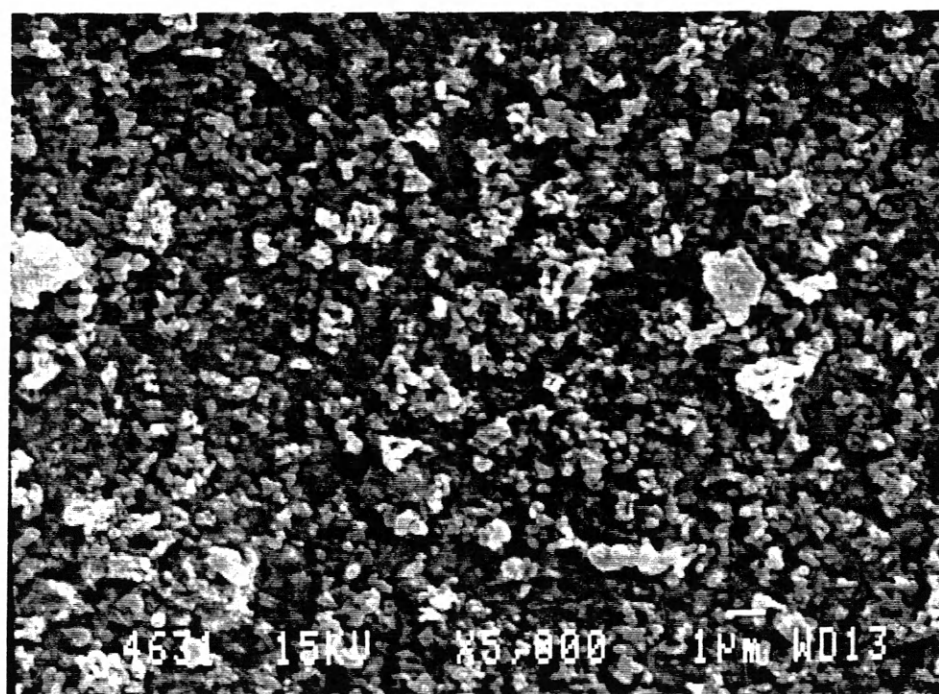
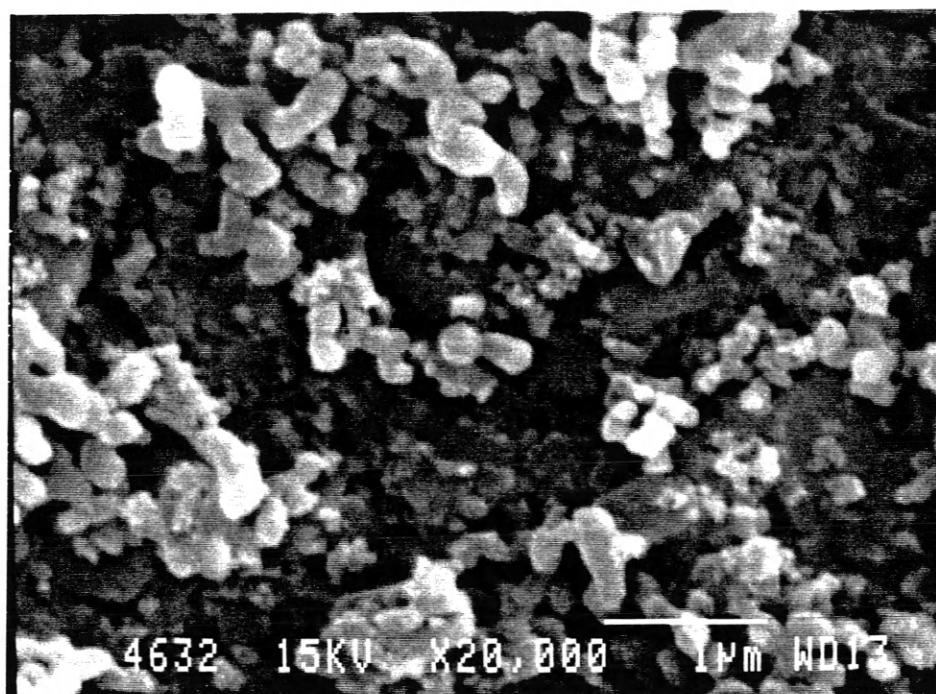


Fig. 5.10 Topography of annealed CdTe 46-3.

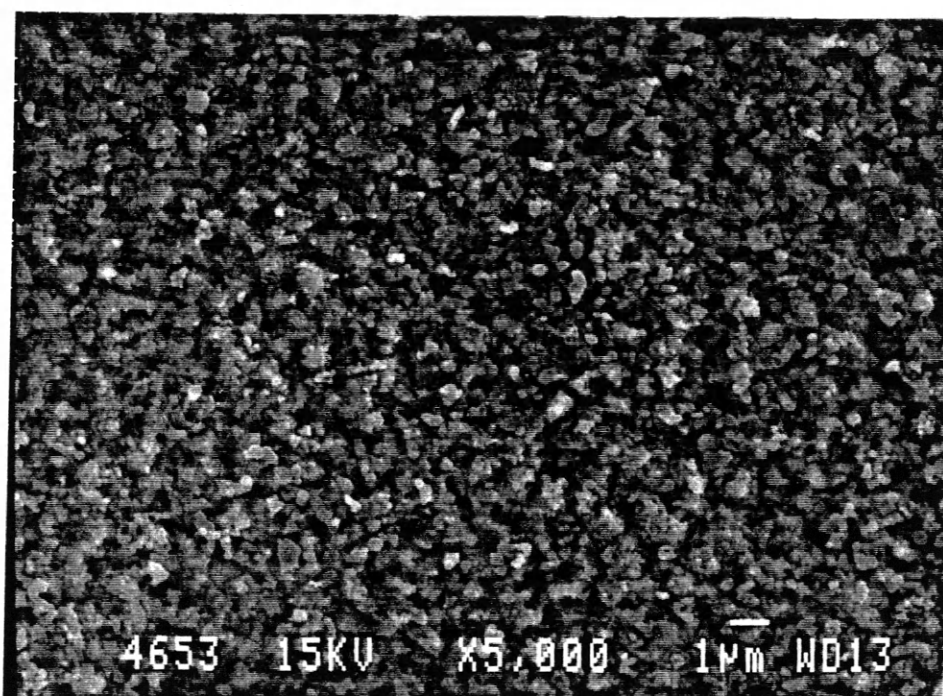
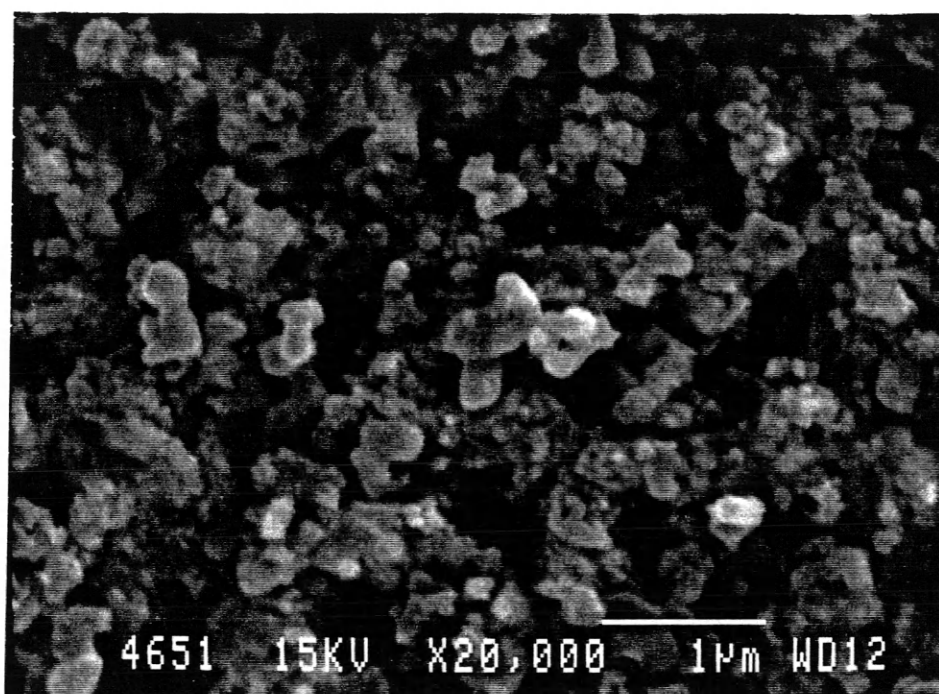


Fig. 5.11 Topography of annealed CdTe 46-5.

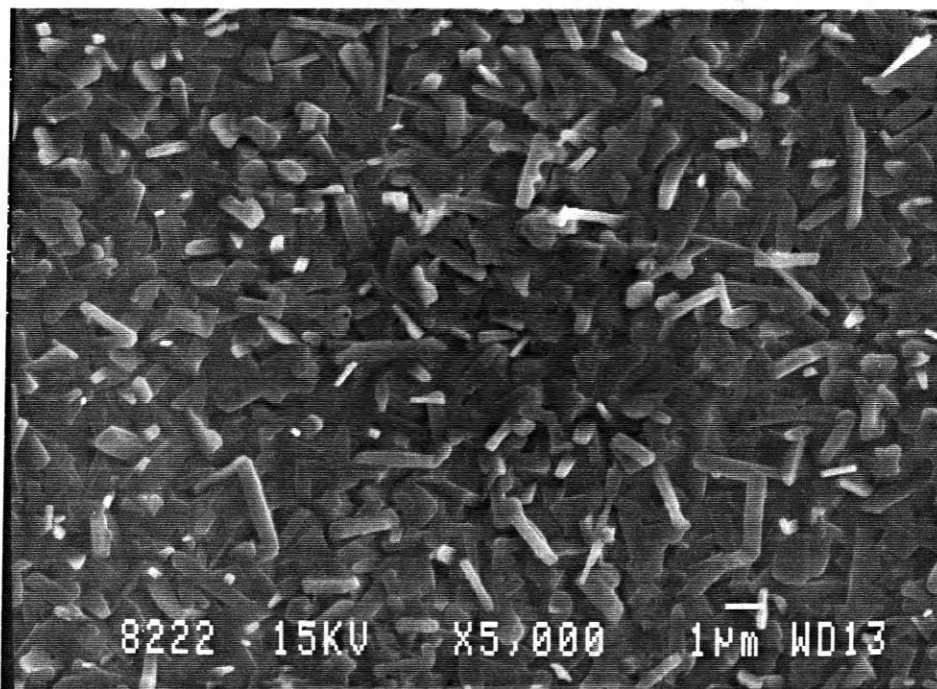
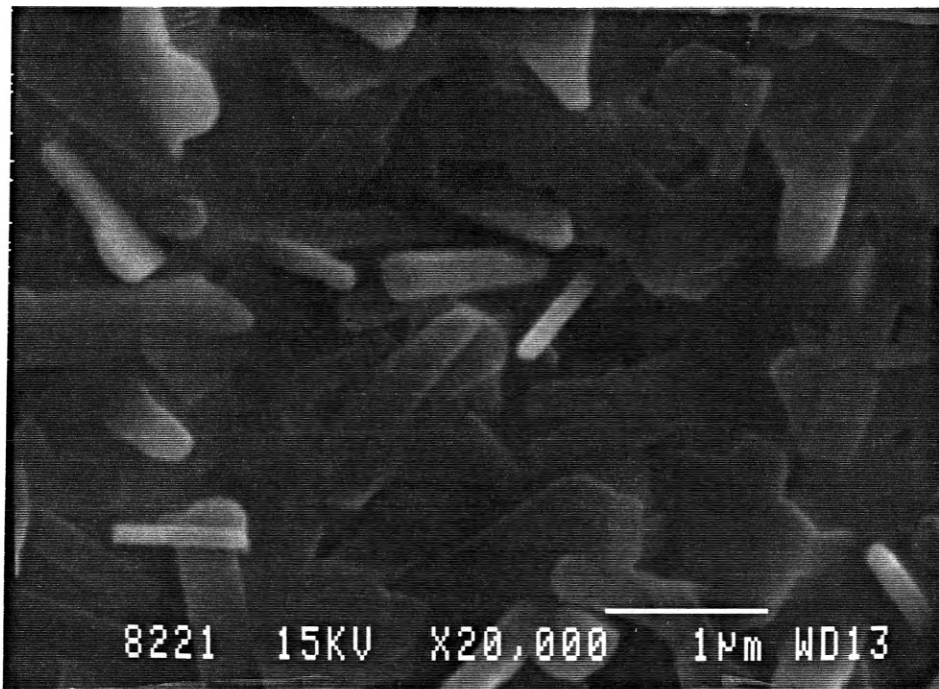


Fig. 5.12 Topography of annealed CdTe 82-2.

5-4. Photoluminescence

A typical photoluminescence spectrum of high quality CdTe consists of two main peaks. A narrow peak occurring at 1.58 eV is attributed to radiation transitions from near band edge states. Another broader peak at 1.4 eV is attributed to deep acceptor-like levels associated with complex centers. A typical spectrum is given in Figure 5.13. [20]

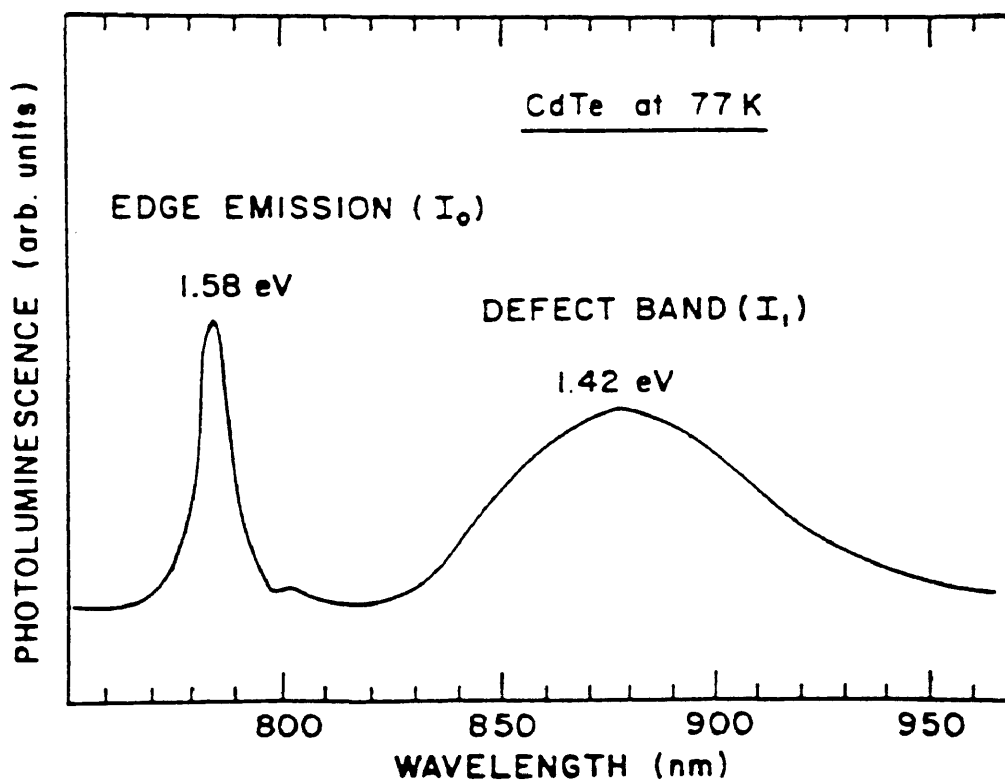


Fig. 5.13 A typical PL intensity spectrum of CdTe at 77 K [20].

According to Giles et al.[20] high quality materials will exhibit bright, narrow edge PL peaks with a low intensity defect band. A radiative defect density ρ was used to measure the quality of the material and is defined as the ratio of the integrated intensity of the defect band I_1 to that of the edge peak I_0 .

The band gap of CdTe is 1.6 eV and 1.5 eV at 0 K and room temperature, respectively [21]. The main interest here is to study the interdiffusion of CdS into CdTe. Room temperature measurements were employed to investigate the band gap for each sample. The results were used to find out how much interdiffusion occurred in the CdTe layer. The results of Ohata et al.[22] were used to correlate the band gap and the CdS ratio in the CdTe layer (See Figure 5.14).

All of the as grown samples displayed one main peak as shown in Figures(5.15-18). Two spectra were collected for Sample 46-6, which was prepared under standard conditions, the second spectrum displayed another peak. In this case however, this peak was very weak. The peaks for sample 46-6 and sample 46-3 are almost at the same energy (1.47 eV) while sample 46-5 has a peak at slightly lower energy (1.44 eV).

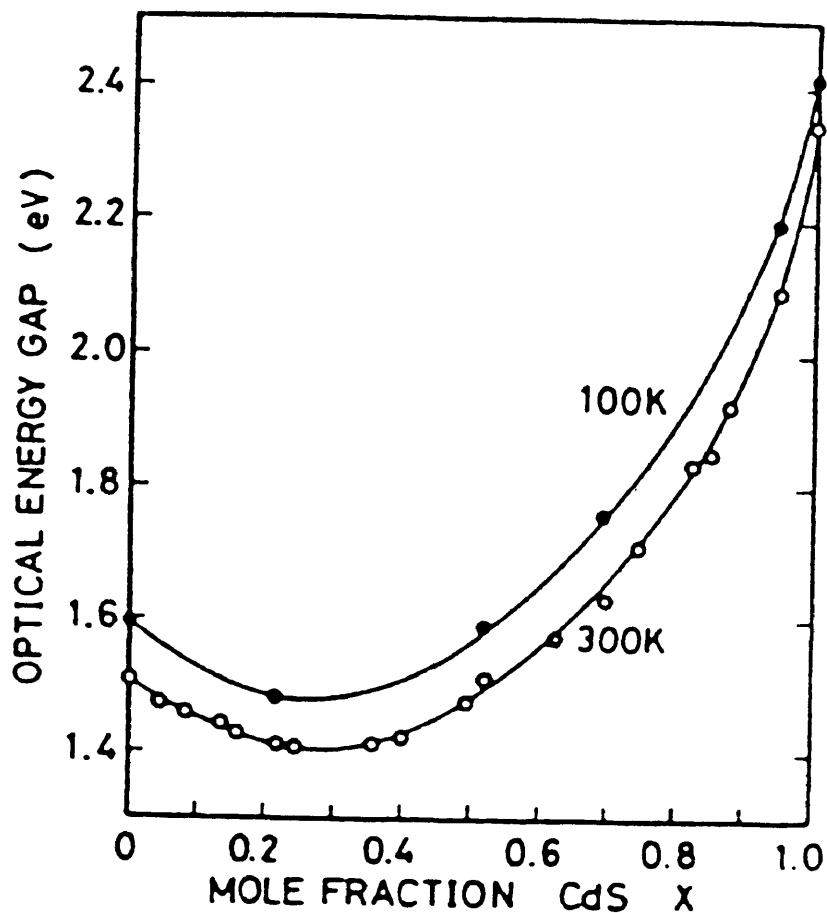


Fig. 5.14 Optical energy gap of $\text{CdS}_x\text{Te}_{1-x}$ at 300K and at 100 K. [22].

For sample 46-5 (See Figure 5.19) the band gap energy was about 1.5 eV which according to Ohata Figure indicates CdTe free of CdS. For sample 46-6 (see Figure 5.20), the measured band gap was about 1.48 eV which means more CdS diffusion into the CdTe (about 4%). This is consistent with the previous results of the CSM CdTe group [23]. For sample

46-3 (Figure 5.21) the band gap energy was about 1.49 eV which gives an indication of some CdS interdiffusion. Using Figure 5.14, this energy will correspond to about 2% CdS diffusing into the CdTe layer.

At 5 K, annealed samples behave differently. Sample 46-5 (Figure 5.22) displayed one broad peak. However after deconvolution of the peak using a software, two defect levels very close to each other ($\Delta E = .02$ eV) were found. They are at 860 nm (1.44 eV) and at 850 nm (1.46 eV). Sample 46-3 (Figure 5.23) has only one defect level at 850 nm (1.46 eV). Sample 46-6 (Figure 5.24) showed a strong defect peak at 863.3 nm (1.43 eV) in addition to another defect peak at 800 nm (1.55 eV). The defect level was deep ($\Delta E = .12$ eV).

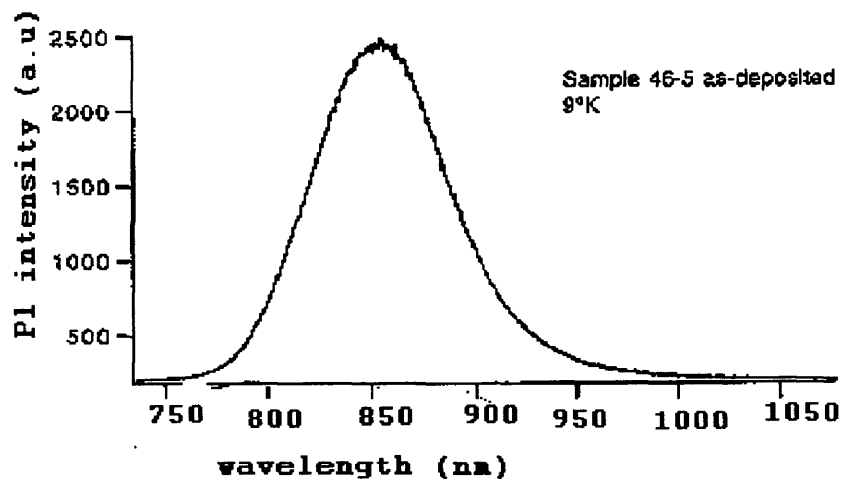


Fig.5.15 PL measurement of as-grown CdTe 46-5.

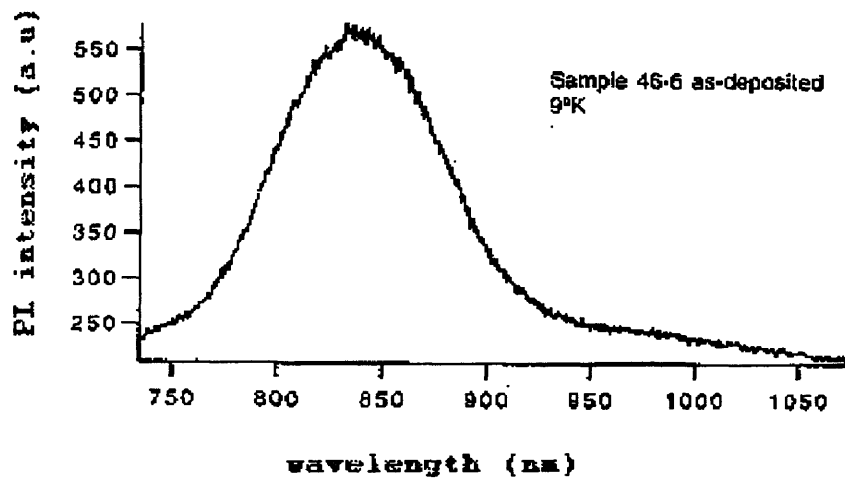


Fig.5.16 PL measurement of as-grown CdTe 46-6

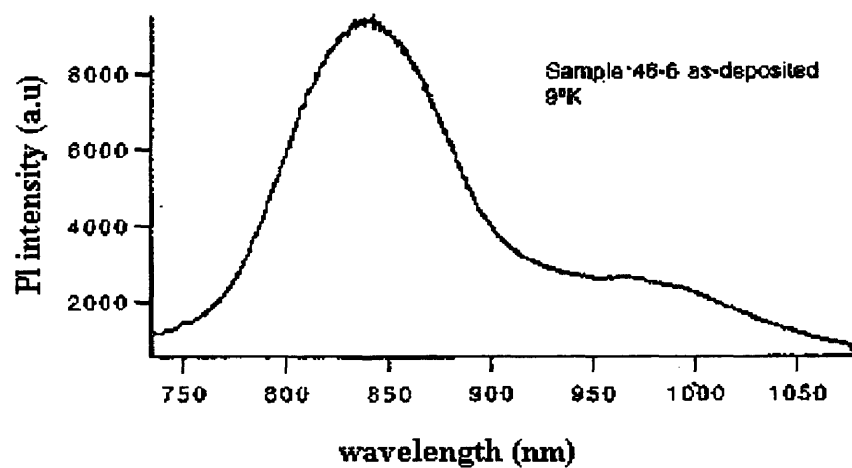


Fig.5.17 PL measurement of as-grown CdTe 46-6

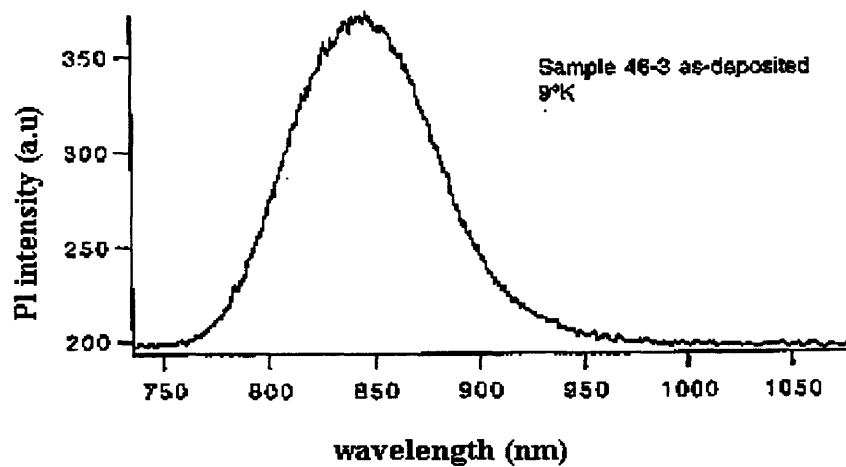


Fig. 5.18 PL measurements of as-grown CdTe 46-3.

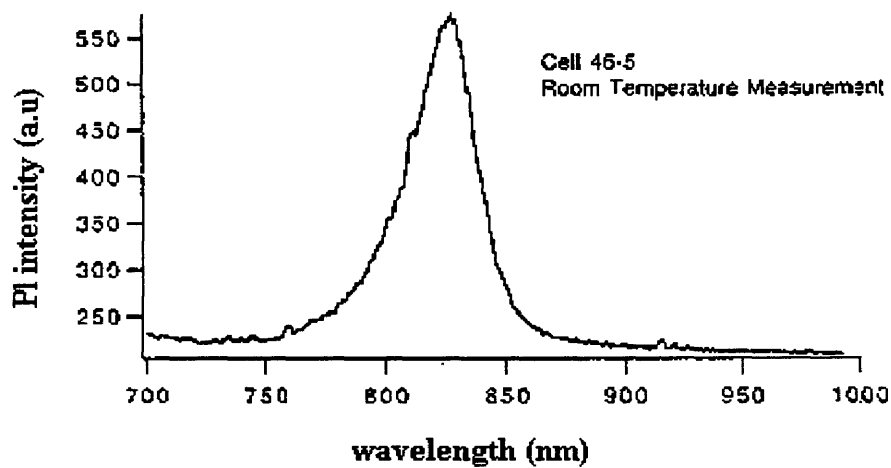


Fig.5.19 PL measurement of annealed CdTe 46-5 at room temperature.

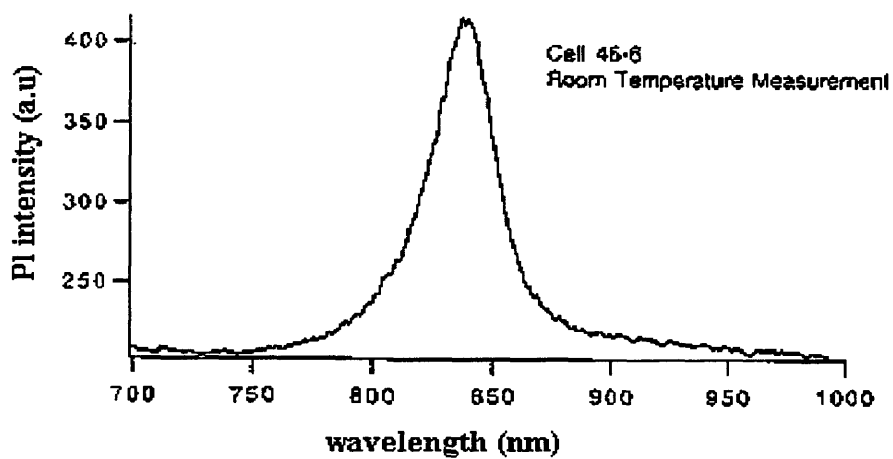


Fig.5.20 PL measurement of annealed CdTe 46-6 at room temperature.

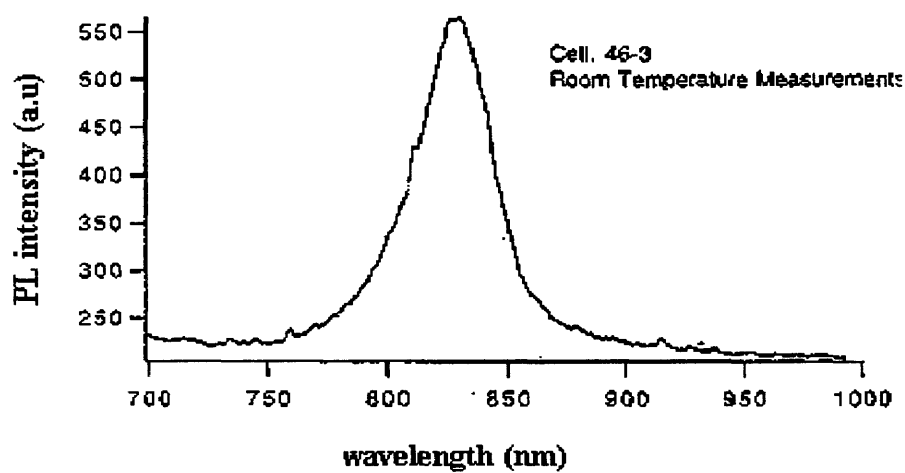


Fig.5.21 PL measurement of annealed CdTe 46-3 at room temperature.

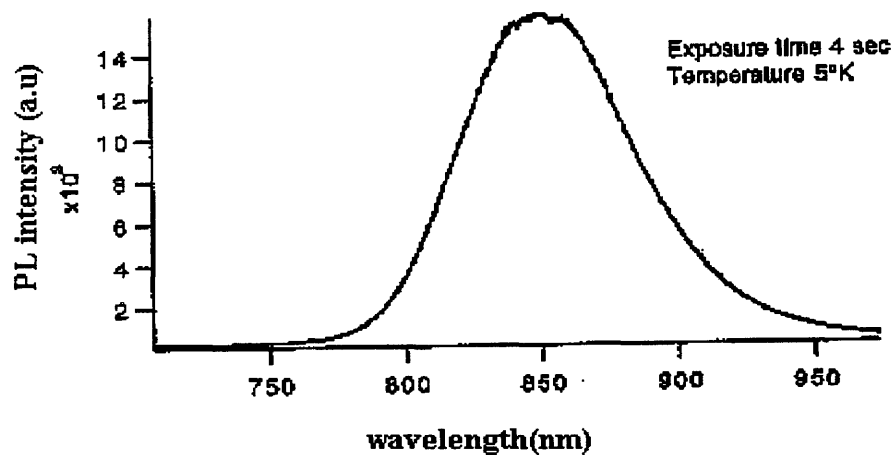


Fig. 5.22 PL measurement of annealed CdTe 46-5 at 5k.

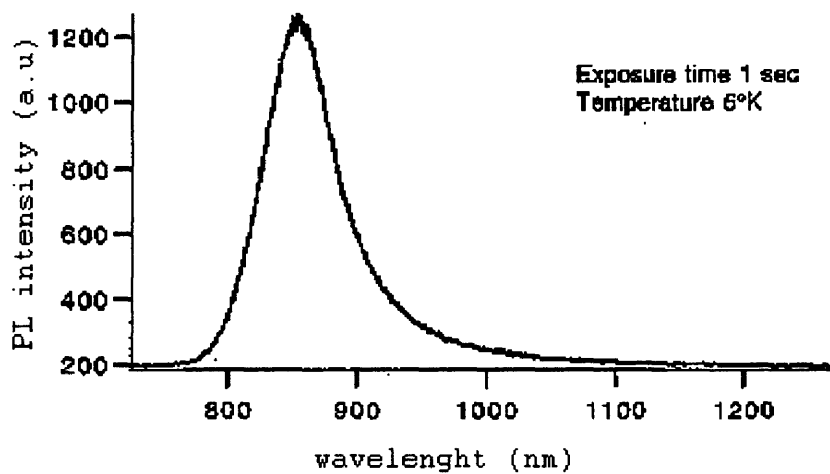


Fig.5.23 PL measurement of annealed CdTe 46-5 at 5k.

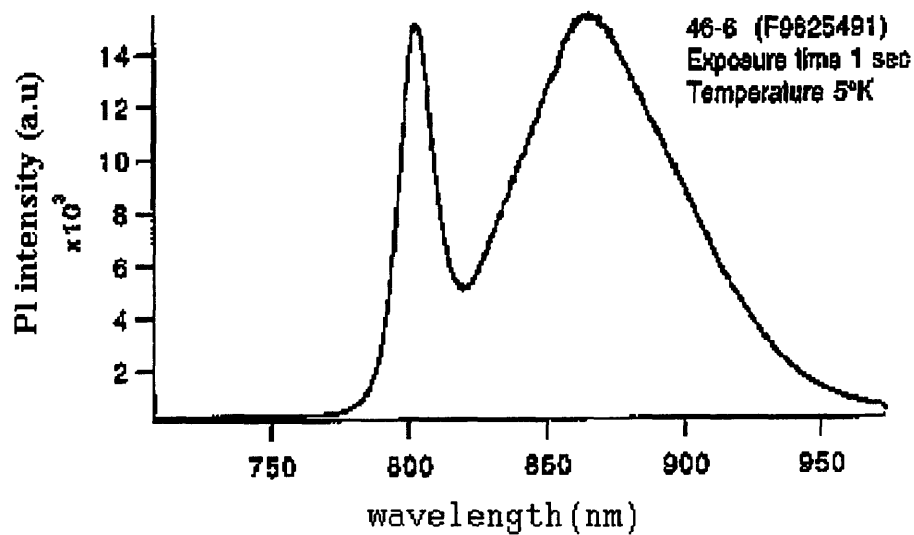


Fig.5.24 PL measurement of annealed CdTe 46-6 at 5k.

5-5 Life Time Measurements

Sample 46-3 gave the highest PL lifetime measurements of 1.54 ns and 0.715 ns in the front (glass side) and the back (ohmic contacts side) respectively. Sample 46-5 was next with lifetimes of 1 ns and 0.17 ns in the front and the back respectively. Sample 46-6 (the standard) had the lowest lifetimes of 0.53 ns and 0.09 ns in the front and in the back respectively (Fig. 5.25).

The results of the above lifetime measurements performed at NREL were comparable to results obtained by other groups [24]. The University of Toledo group obtained decay lifetimes of 0.5 ns and 0.3 ns for CdTe/CdS cells in the front and in the back respectively [25]. The University of South Florida has reported lifetimes ranging from 0.4 ns to 1.5 ns [25].

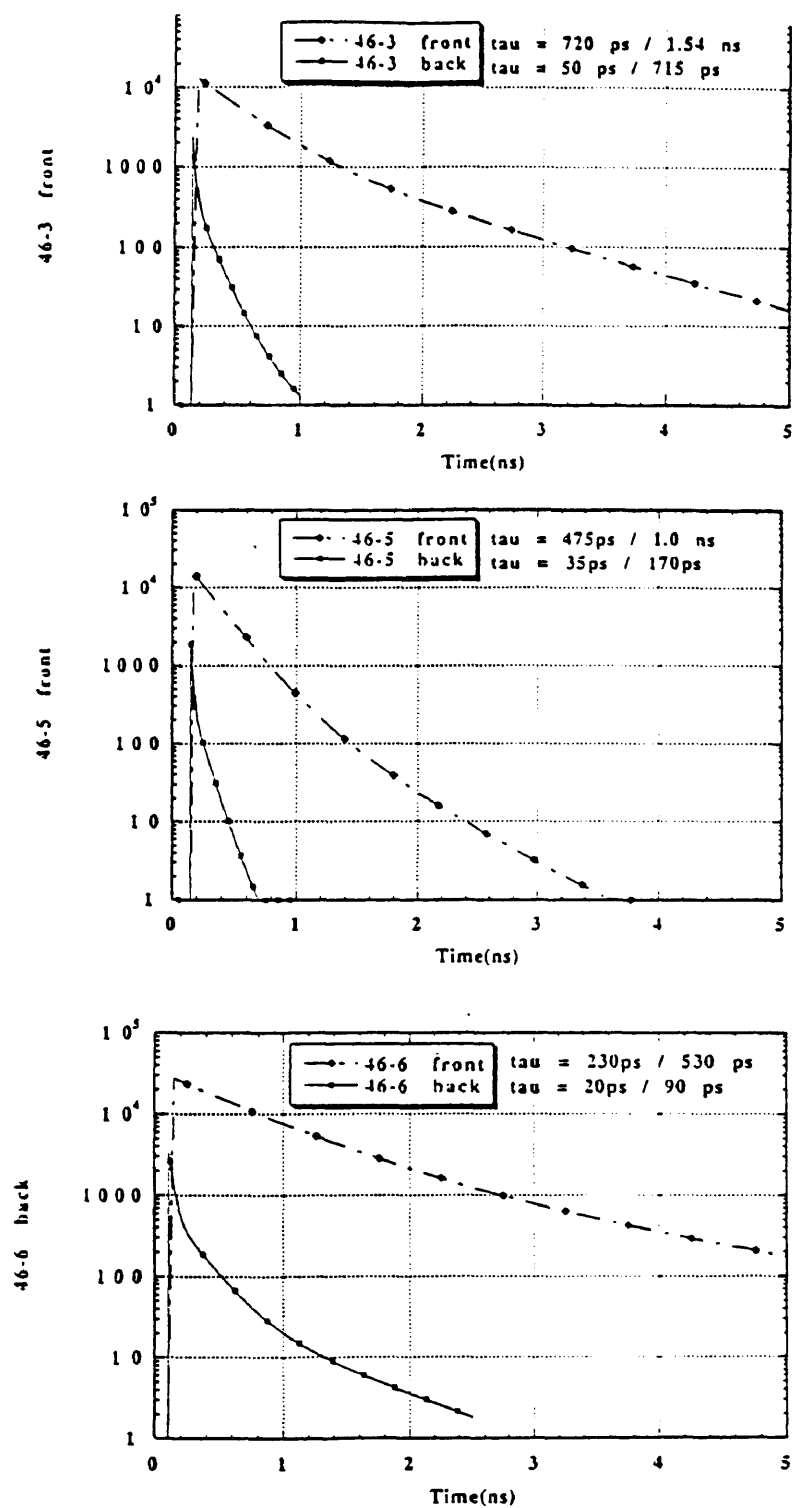


Fig. 5.25 lifetimes of the three samples of CdTe.

5-6 Auger Electron Spectroscopy Results

The AES results provided significant information for studying the interdiffusion in the samples. In the as-grown sample 46-5 (see Figures 5.26-29), the line scan indicated that very little Te and S had diffused into the CdS and CdTe respectively. As can be seen in fig.5.26 the Te concentration formed a slight dip before reaching the interdiffusion region. The same dip was observed in the Cd concentration and is an artifact of the measurements. Relative to the Cd peak in CdS, the Cd peak in CdTe (fig.5.27) is shifted by about 1 eV towards higher energy. This result is consistent with the standard Cd peak values for these materials [26]. The energy of the Cd peak in the interface is different from both the Cd peaks in the CdTe or CdS regions. This could not be accounted for as a broad peak which could result if aggregates of both CdS and CdTe were present at the interface. Instead we conclude that there is a ternary alloy of $\text{CdTe}_{1-x}\text{S}_x$ at the interface which is also consistent with the line scan results.

After annealing of sample 46-5 (Figures 5.30-32) the Auger line scans indicated that only a small amount of Te diffused into the CdS. On the other hand, almost no S diffused into the CdTe. This is consistent with the PL measurement results. Also, the energy of the Cd peak in the

interface coincides with that of the Cd peak in CdTe which means that little diffusion is present.

For the as-grown state of sample 46-6 (Figure 5.33-36) the Cd peak in CdTe is shifted towards higher energy than in CdS. However, this shift is less than the 1.1 eV which is the standard case [26]. Its magnitude of about 0.5 eV may be indicative of diffusion. The Cd peak is also shifted at the interface which may indicate the existence of ternary alloy, $\text{CdTe}_{1-x}\text{S}_x$, at the interface.

After annealing the sample 46-6 (fig.5.37-39), the Cd peak in the interface is shifted towards higher energy than the Cd peak in CdTe which also is an indication of the existence of ternary alloy in the interface instead of a mixture of CdS and CdTe.

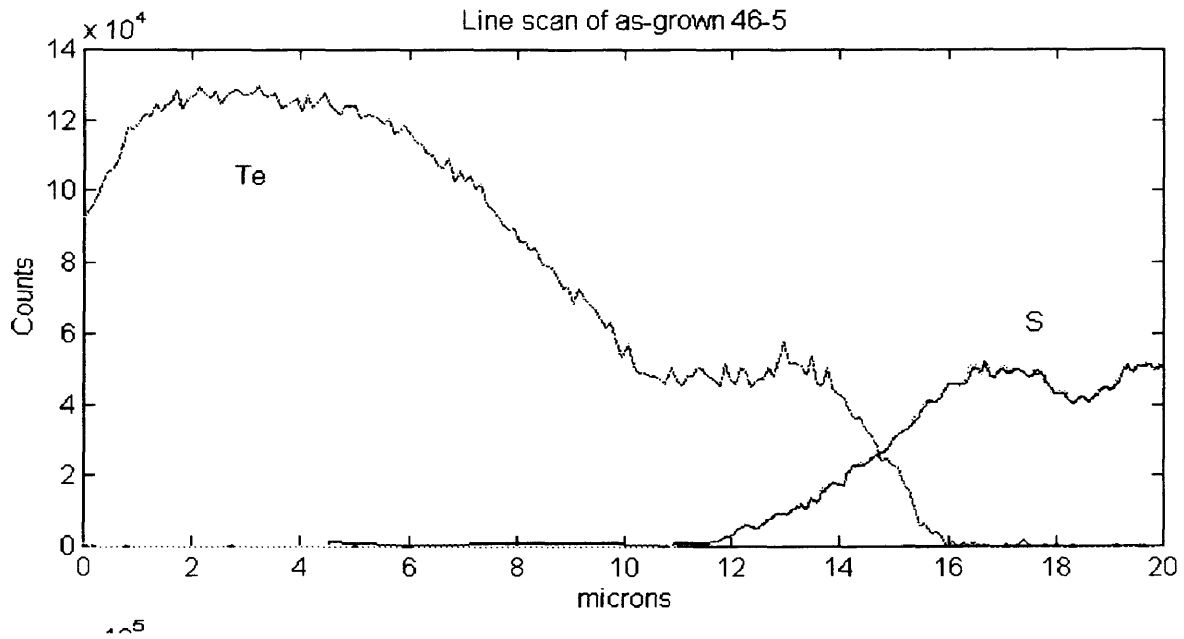


Fig. 5.26 Line scan of the as-grown sample 46-5.

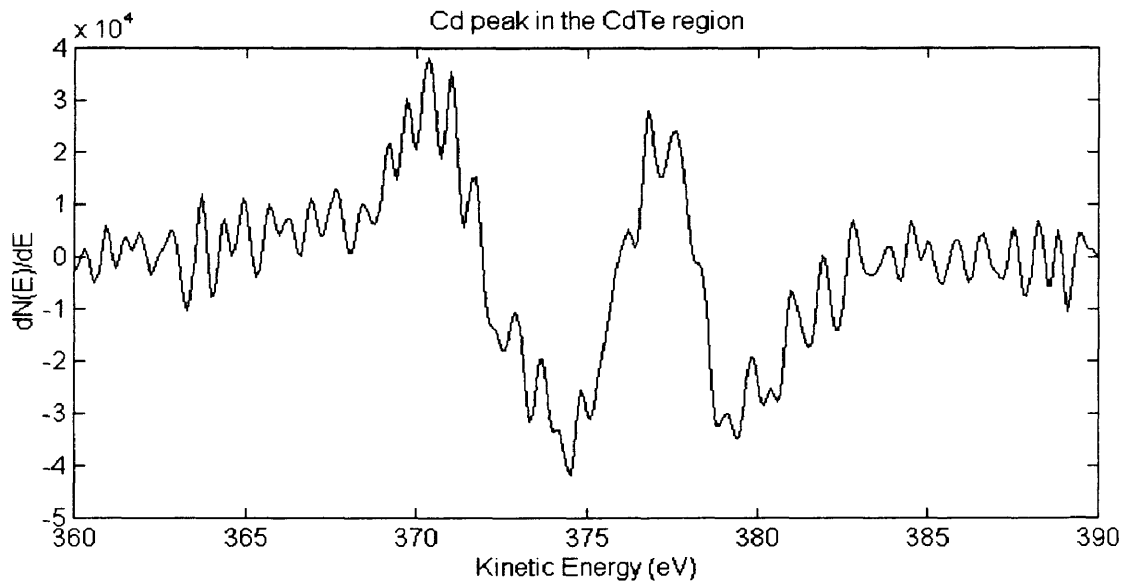


Fig 5.27 Cd peak in the CdTe region for as-grown 46-5.

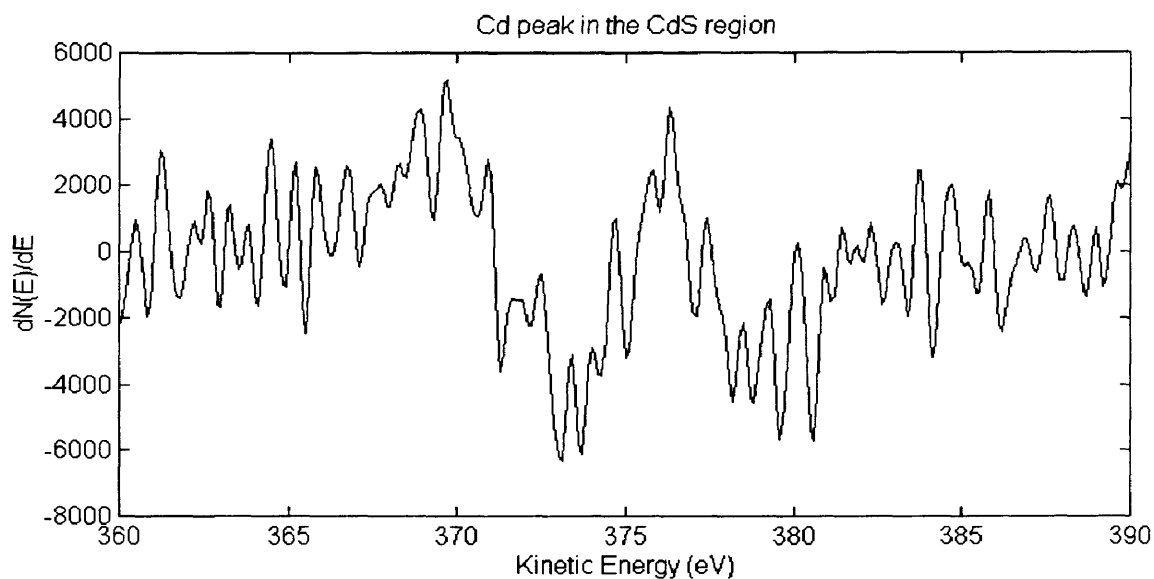


Fig. 5.28 Cd peak in the CdS region for as-grown 46-5.

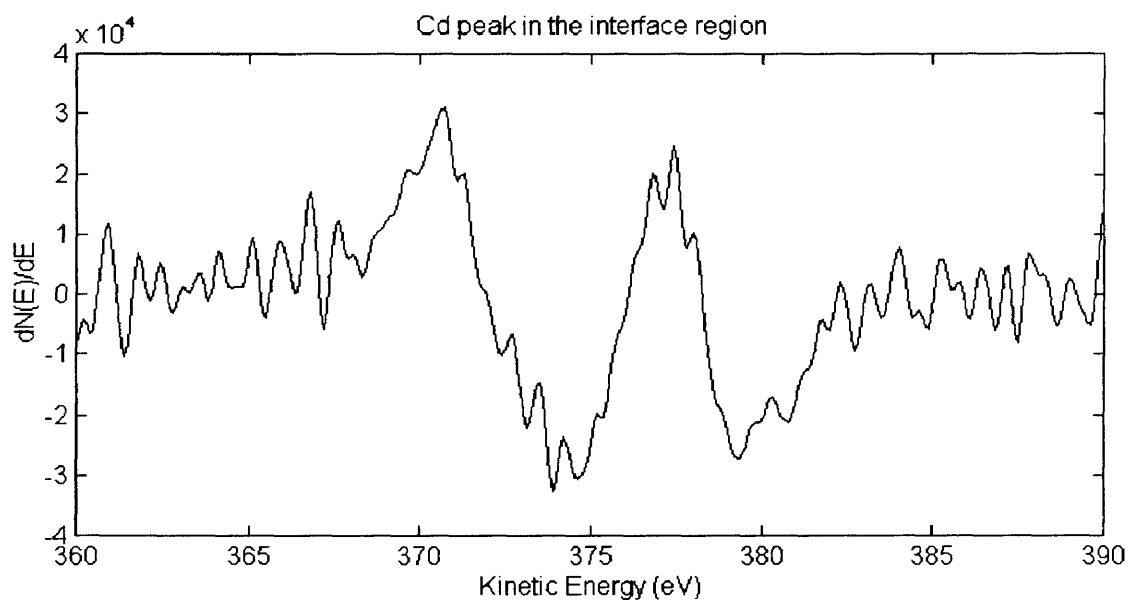


Fig. 5.29 Cd peak in the interface for as-grown 46-5.

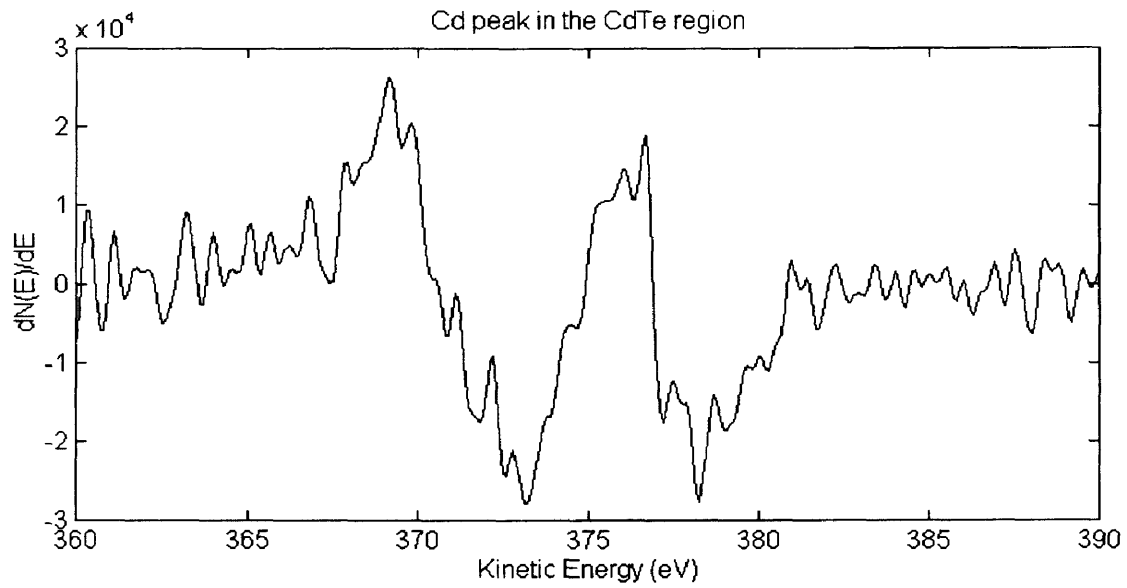


Fig. 5.30 Cd peak in the CdTe region for annealed 46-5.

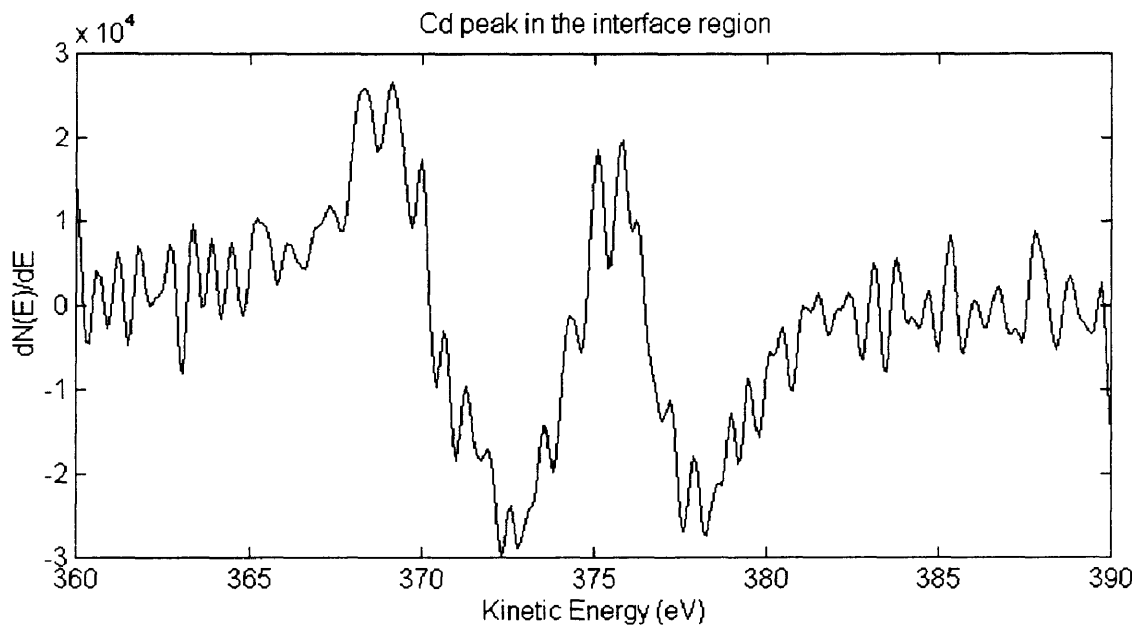


Fig. 5.31 Cd peak in the interface for annealed 46-5.

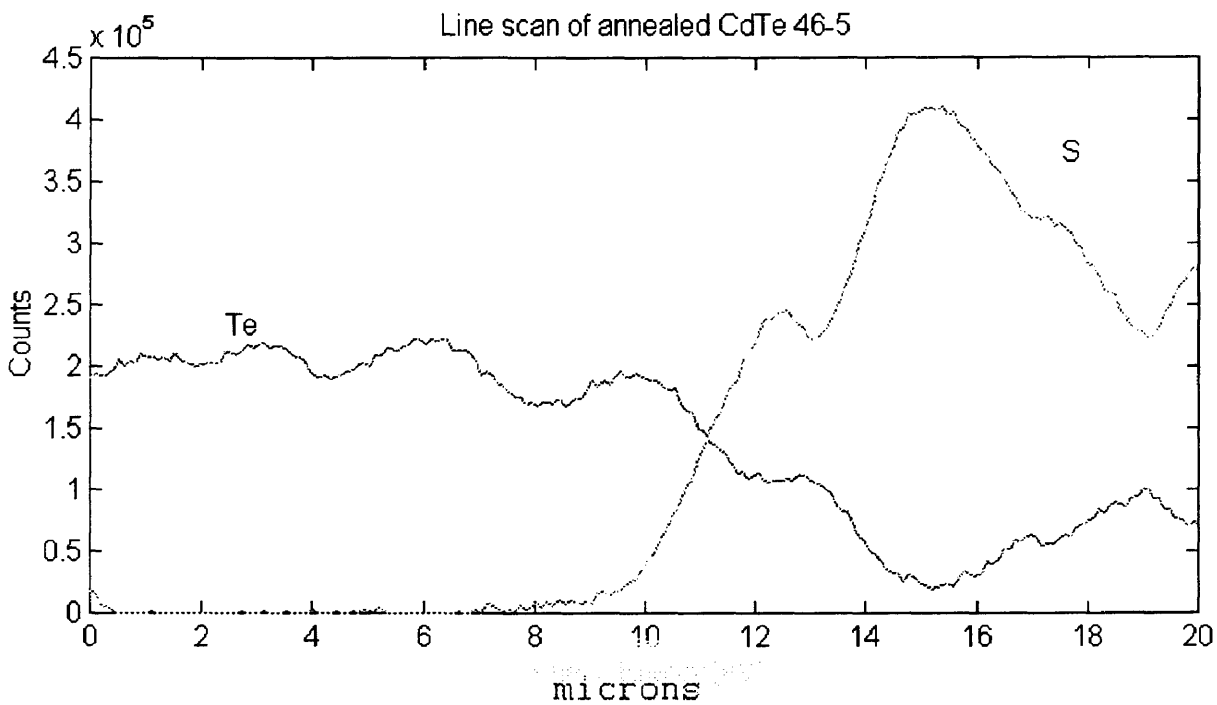


Fig. 5.32 line scan for annealed 46-5.

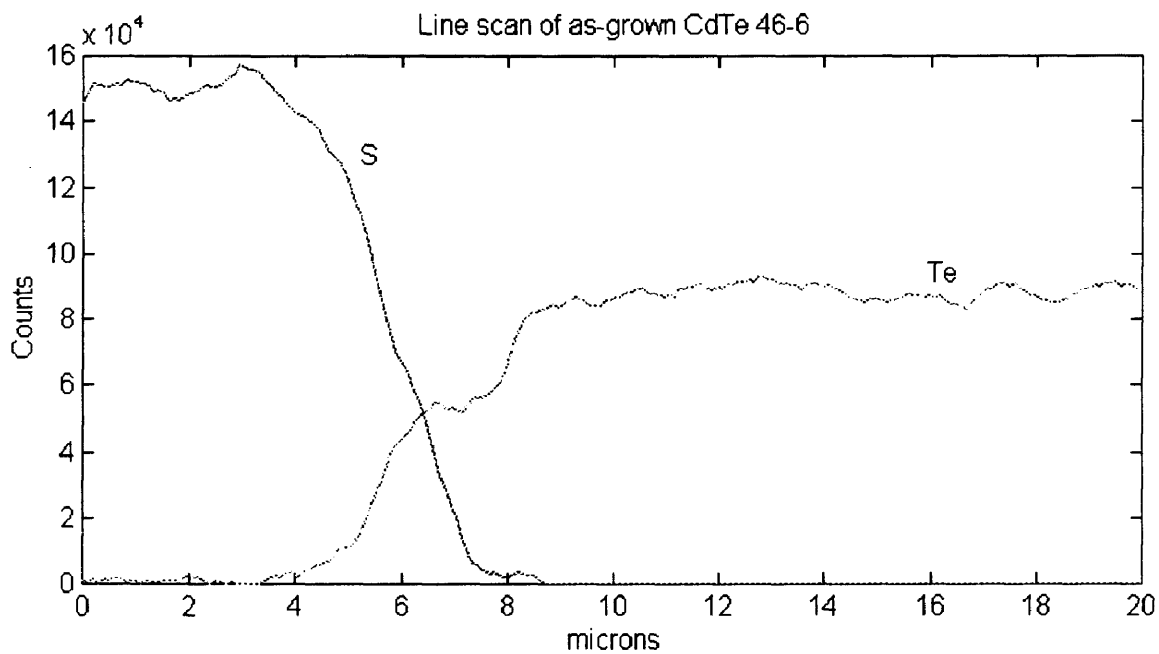


Fig. 5.33 line scan for as-grown 46-6.

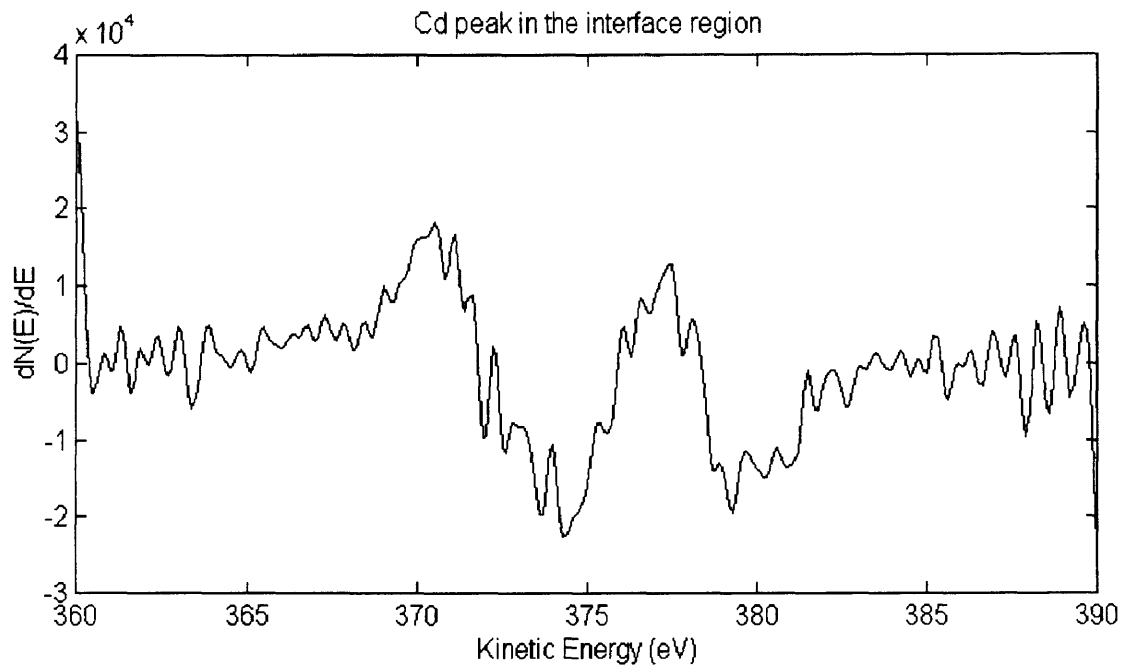


Fig. 5.34 Cd peak in the interface for as-grown 46-6.

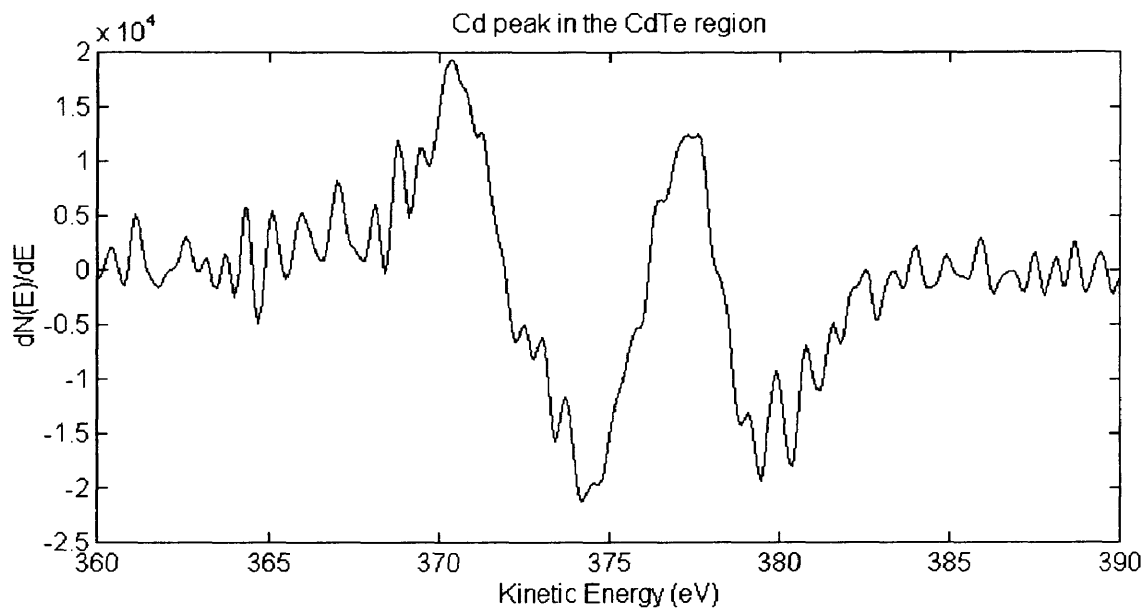


Fig. 5.35 Cd peak in the CdTe region for as-grown 46-6.

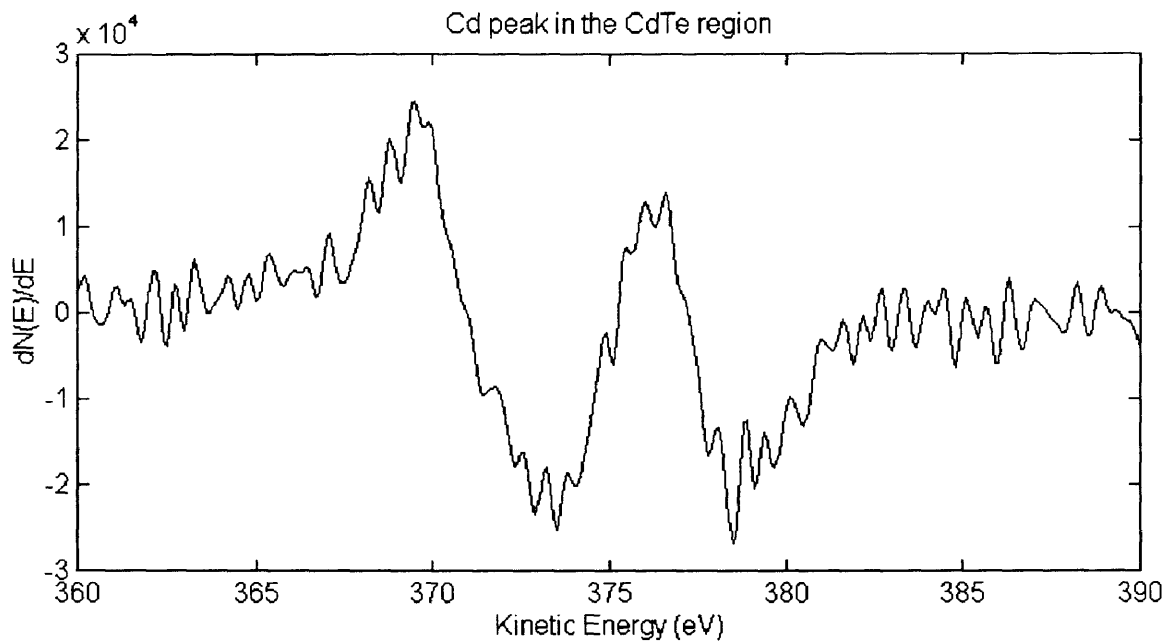


Fig. 5.36 Cd peak in the CdTe region for as-grown 46-6.

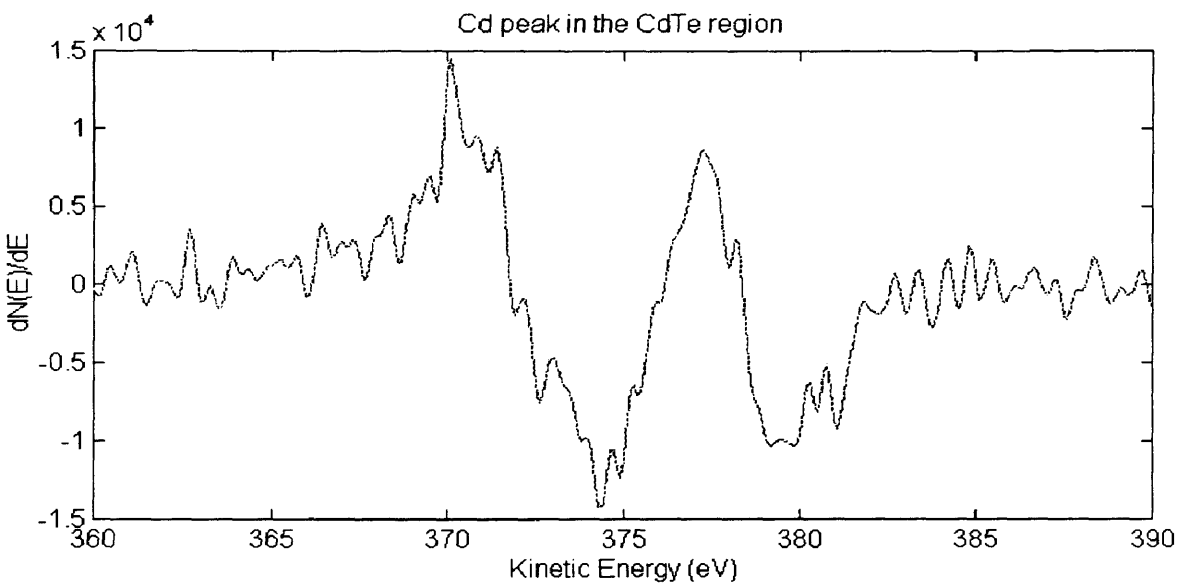


Fig. 5.37 Cd peak in the CdTe region for annealed 46-6.

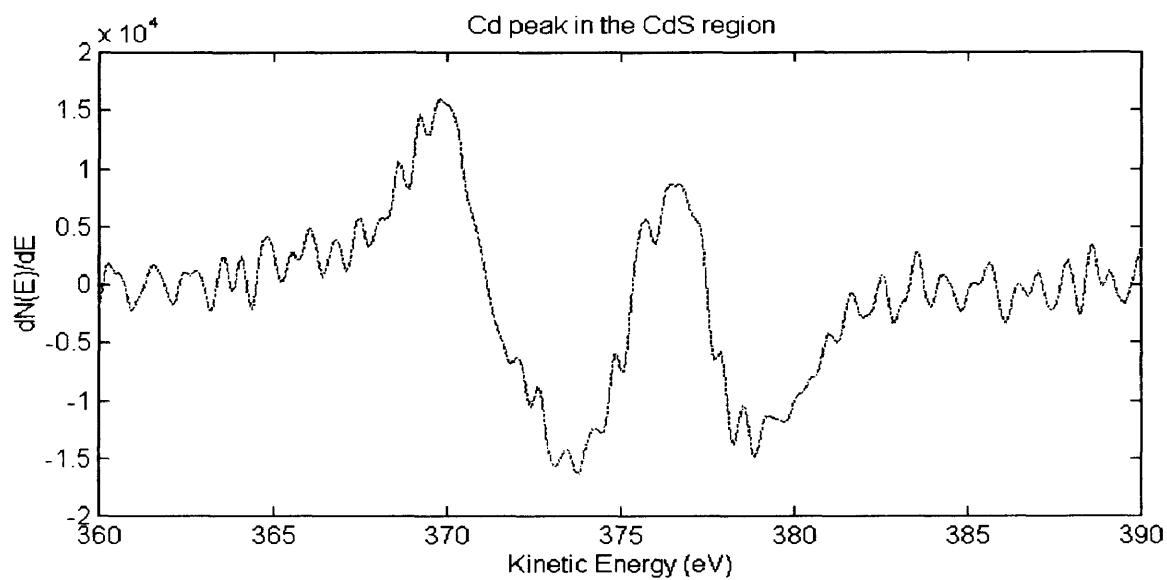


Fig. 5.38 Cd peak in the CdS region for annealed 46-6.

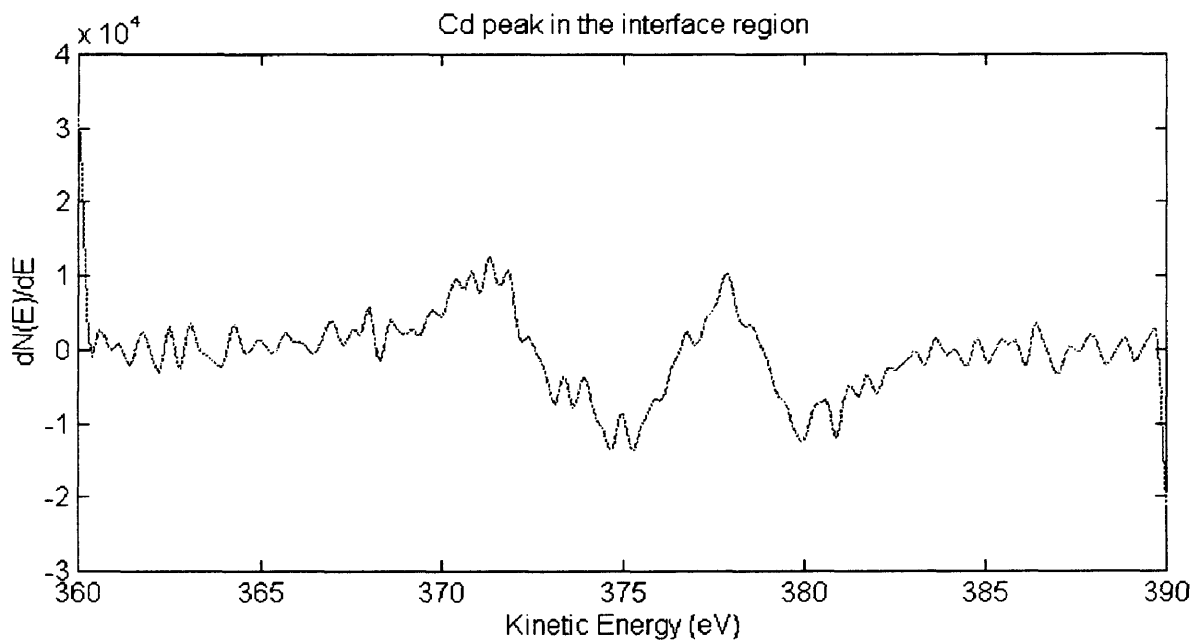


Fig. 5.39 Cd peak in the interface for annealed 46-6.

5-7 Efficiency Measurements

Below is a table summarizing the efficiency measurements of all the samples. It is clear that the graded potential sample(82-2) has the highest efficiency and short circuit current. The standard sample (46-6) has the next highest efficiency.

Table 5.14 Efficiencies of the different samples of CdTe.

Sample	efficiency (%)	FF(%)	V_{oc} (mV)	J_{sc} (mA) / cm^2
46-5	7.8	50	720	21.7
46-3	7.9	53	710	21.0
46-6	9.7	63	695	22.0
82-2	10.8	58	765	24.3

CHAPTER 6

SUMMARY AND CONCLUSIONS

In the as-deposited state, the three samples, 46-5, 46-3 and 82-2, displayed similar texture in the [111] direction. All these samples had stronger texture than sample 46-6. After annealing, samples 46-6 and 82-2 had the strongest texture with the (220) peak being the dominant peak.

With regard to grain size, "fabrication of high efficiency devices requires that the CdTe grain size be ≥ 1 μm in order to avoid significant surface recombination associated with large interface state density" [24]. Sample 82-2 had the highest grain size of about 1.5 μm . The grain size of sample 46-5 was the smallest. This might be correlated to the interdiffusion since smaller grains are packed more closely, and less interdiffusion might take place.

Concerning lifetime measurements, sample 46-6 displayed the shortest lifetime, while sample 46-3 showed the highest lifetime. In addition, Auger measurements showed that

sample 46-6 had appreciable interdiffusion while sample 46-5 had very little. This result was confirmed by the PL measurements at room temperature.

Sample 82-2 had the highest efficiency, short circuit current, and open circuit voltage among all the samples but its fill factor was lower than that of sample 46-6. Sample 46-6 had the highest fill factor (63), but was close to sample 82-2 in all other parameters.

One conclusion from the present work is that improved junctions may be formed by grading the deposition potential. By making a graded potential sample, starting at the lowest potential and moving higher during deposition, many advantages can be achieved. First, interdiffusion from CdS to CdTe and vice versa can be minimized since we start from the lowest deposition potential, which leads to a minimum interdiffusion. Second, grain sizes can be improved. In addition, by varying the potential, a graded junction might be obtained which will enhance the performance of the cell, This was clear from the high short circuit current obtained from sample 82-2 which was higher than the short circuit current from the samples prepared at fixed deposition potential.

REFERENCES CITED

1. Neville, Richard c. 1978. Solar Energy Conversion: The Solar Cell Netherlands: Elsevier: 22-26.
2. Zweibel, Ken. 1990. Harnessing Solar Power New York: Plenum Press: 2.
3. Zweibel, Ken. 1990. Harnessing Solar Power New York: Plenum Press: 181.
4. Panicker, M.P.R., Kanster, M. and Kroger, F .A 1978
Cathodic Deposition of CdTe From Aqueous Electrolytes
J.Electrochem Soc. (April) :125(4) ,566-572.
5. Takahashi, Makoto Uoski, Kohei and Kita, Hideaki 1984
Electrochemical Deposition , Optical Properties, and
Photoelectrochemical Behavior of CdTe Films ,J.Electrochem Soc., 131(10), 2304-2307.
6. Cowche, Pierre, Lincot, Daniel and Vedel, Jacques 1989
Cathodic Codeposition of Cadmium Telluride on Conducting
Glass J.Electrochem Soc. 136(6): 1646-1649.
7. Sella, Catherine, Boncorps, Pascale and Vedel, Jacques
1986 The Elecrtodeposition Mechanism Of CdTe from Acidic
Aqueous Solutions J.Electrochem Soc 133(10): 2043-2047.
8. Kampmann, A., Cowache, P., .Mokili, Lincot, D., .Vedel, J
1995 Characterization of [111] cadmium telluride

electrodeposited on cadmium sulphide Journal of Crystal Growth 146: 256-261.

9. Meyers, Peter V. 1988 Ametek CdTe Solar Module Development Program Solar Cells 24:35-42.

10. Cullity, B.D 1978 Elements OF X-ray Diffraction Addison Wesley Publishing CO.INC. :295-300.

11. Fahrenbruch , Alan L. and Bube, Richard H. 1983. Fundamentals OF Solar Cells Academic Press.

12. Raub, E. and Muller, K. 1967. Fundamentals OF Metal Deposition Netherland: Elsevier Publishing CO.

13. Stradling, R A, Klipstein, P.C. 1991 Growth and Characterization of Semiconductors Bristol England Adam Hilger: 135-140.

14. Schroder, Dieter. 1990. Semiconductor Material and Device Characterization John Wiley & Sons

15. Carlson, T.A 1975 Photoelectron and Auger Spectroscopy New York: Plenum.

16. Pozder, Scott 1995 Effects of Cadmium Telluride Electrodeposition Parameters on the Efficiency of Cadmium Sulfide/Cadmium Telluride/Gold Solar Cell Thesis CSM

17. Lea, C. and Seah, M.P. 1981 Optimized Depth Resolution in Ion-Sputtered and Lapped Compositional Profiles with Auger Electron Spectroscopy Thin Solid Films 75:67-86.

18. Abou-Elfotouh, F.A. and Coutts, T.J. 1992 RF Planar Magnetron Sputtering of Polycrystalline CdTe Thin-Film solar Cells. Int J. Solar Energy 12:223-231.
19. Mader, Siegfried 1970 Determination OF Structure in Films IN Handbook OF Thin Film Technology Edited by Leon I Maissel and Reinhard Glang, McGRAW-HILL, New York: P 9-1-10-1.
20. Giles, Taylor, N.C, Bicknell, R.N Blanks, D.k. Myers, T.H. and Schetzina, J.F. 1985 Photoluminescence of CdTe:A comparison of bulk and epitaxial material J.Vac.Sci.Technol 3(1):76-82.
21. Pankove, Jacques I. 1971. Optical Processes in Semiconductors New York: Dover Publications, Inc:412
22. Ohata, Keichi, Saraie, Juni 1973 Optical Energy Gap of the Mixed Crystal CdS_xTe_{1-x} Japan.J.Appl.Phys 12(10):1641-1642.
23. Mao, D , Feng, L.H Zhu, Y. Tang, J. Song, W. Collins, R. Williamson, D.L. and Trefny, J.U.. 1995 Interdiffusion in polycrystalline Thin-Film CdTe/CdS Solar Cells. 13th NREL Photovoltaic Program Review Meeting, Lakewood Co. May.
24. Nelson, Art , F. Hason, and Dean Levi 1994 Processing and characterization of large-grain thin-film CdTe J.Vac.Sci.Technol. 12(5):2803-2807.

25. Compaan, Alvin, Tabory, Charles N. Yuxin Li, Zhirong Feng, and Fischer, Andreas 1993 CdS/CdTe solar cells by sputtering and by laser physical vapor deposition 24th IEEE Photovoltaic Specialist Conference :394-399.
26. Briggs, D., and Seah, M.P. 1990 Practical surface Analysis(second edition); Volume 1:Auger and X-ray Photoelectron Spectroscopy John Wiley & Sons:614.